Searches for dark matter decay with ultrahigh-energy neutrinos endure backgrounds

Damiano F. G. Fiorillo[1,*], Víctor B. Valera,[1,†] Mauricio Bustamante[1,‡] and Walter Winter[2,‖]

[1]*Niels Bohr International Academy, Niels Bohr Institute, University of Copenhagen,*
2100 Copenhagen, Denmark
[2]*Deutsches Elektronen-Synchrotron DESY, Platanenallee 6, 15738 Zeuthen, Germany*

Next-generation ultrahigh-energy (UHE) neutrino telescopes, presently under planning, will have the potential to probe the decay of heavy dark matter (DM) into UHE neutrinos, with energies in excess of 10^7 GeV. Yet, this potential may be deteriorated by the presence of an unknown background of UHE neutrinos, cosmogenic or from astrophysical sources, not of DM origin and seemingly large enough to obscure the DM signature. We show that leveraging the angular and energy distributions of detected events safeguards future searches for DM decay against such backgrounds. We focus on the radio detection of UHE neutrinos in the planned IceCube-Gen2 neutrino telescope, which we model in state-of-the-art detail. We report promising prospects for the discovery potential of DM decay into UHE neutrinos, the measurement of DM mass and lifetime, and limits on the DM lifetime, despite the presence of a large background, without prior knowledge of its size and shape.

I. INTRODUCTION

About 85% of the matter in the Universe is dark, not interacting electromagnetically nor strongly. Evidence for dark matter (DM) comes from velocity dispersion and rotation curves in galaxies and galaxy clusters [1–5], gravitational lensing measurements in galaxy clusters and collisions of galaxy clusters [6,7], the cosmic microwave background (CMB) anisotropy, and the large-scale structure of the Universe [8–12]. Because this evidence relates to the gravitational effect that DM has on the visible Universe, it provides little guidance to understand other possible interactions between DM and Standard Model particles that could reveal its nature.

The absence of such guidance has spurred a broad program to understand the nature of DM, from theory and experiment. From theory, diverse candidates have been proposed as DM constituents; see, e.g., Ref. [13] for an historical review. These include novel particles, such as weakly interacting massive particles [14,15], axions [16], Majorons [17–19], and sterile neutrinos [20], and non-particle candidates, such as primordial black holes [21]. From experiment, searches for these candidates follow four complementary strategies: collider searches, which attempt to produce DM in high-energy particle collisions; direct DM searches, which look for Galactic DM scattering on dense detector targets; astrophysical searches, which look for the impact that DM would have on cosmic particles; and indirect DM searches, which look for products of DM self-annihilation or decay.

We focus on indirect searches for the decay of heavy DM particles, with masses in excess of 10 PeV, into neutrinos. Our choice is motivated by upcoming experimental capabilities (more on this later) that, for the first time, could allow us to probe DM decay using ultrahigh-energy (UHE) neutrinos, with energies in excess of 10 PeV. (We do not consider DM self-annihilation because, for heavy DM, its cross section is strongly constrained by unitarity bounds [22–24].)

Already in the last decade, the breadth of DM indirect searches widened after the discovery by the IceCube neutrino telescope of high-energy neutrinos of cosmic origin, with energies between 10 TeV and 10 PeV [25–31]. In fact, initially the discovery led to speculation that heavy DM decaying to neutrinos could explain their flux in the 10–100 TeV range [32–43]. Nowadays, more conventional astrophysical explanations are favored [44–47], but IceCube observations still set competitive bounds on the DM lifetime and self-annihilation cross section for DM masses below 10 PeV [48–50]. These bounds are complementary to the ones obtained from gamma-ray observations in a similar mass range; see, e.g., Refs. [48,51,52].

In the next decade, a host of new neutrino telescopes, presently in different stages of planning, design, and prototyping, will target the long-sought discovery of

[*]damiano.fiorillo@nbi.ku.dk
[†]vvalera@nbi.ku.dk
[‡]mbustamante@nbi.ku.dk
[‖]walter.winter@desy.de

UHE neutrinos, between 100 PeV and 10 EeV, that were first predicted in 1969 [53]. They include AugerPrime [54], BEACON [55], EUSO-SPB2 [56], GCOS [57], GRAND [58], POEMMA [59], PUEO [60], RNO-G [61], TAROGE [62], and the radio array of IceCube-Gen2, the envisioned upgrade of IceCube [63]. Ultrahigh neutrinos will bring new insight into astrophysics [64–66] and fundamental physics [65–70]. In particular, they will allow us to test the decay of heavier DM particles, with masses from 10 PeV to 100 EeV; see, e.g., Refs. [24,48,71].

However, the capacity of UHE neutrino telescopes to probe DM decay critically depends on an unknown quantity: the diffuse flux of UHE neutrinos that do not originate from DM decay, and that acts as a background to DM searches. If this background is large, then it could obscure more subtle signatures of neutrinos from DM decay. These background neutrinos—hereafter dubbed "non-DM neutrinos"—are expected from the interaction of ultrahigh-energy cosmic-rays (UHECRs) with ambient matter or radiation inside the extragalactic astrophysical sources where they are accelerated—i.e., *astrophysical* neutrinos—or with cosmic photon backgrounds during their propagation to Earth—i.e., *cosmogenic* neutrinos [53,72,73]. We expand on them later (Sec. II A).

The situation is worsened by the large variety, in size and shape, in the current theoretical predictions of UHE astrophysical and cosmogenic neutrino fluxes; see, e.g., Fig. 2 in Ref. [74]. Without a firm estimate of the non-DM UHE neutrino background, it would seem that the mere discovery of UHE neutrinos may be insufficient to establish whether they originate from DM decay or not. Were the possibility of a background of non-DM UHE neutrinos ignored, the evidence for or against DM decay could be interpreted erroneously.

We show that these difficulties can be overcome by leveraging known differences between the distributions in energy and arrival directions of UHE neutrinos from DM decay and non-DM UHE neutrinos. Regarding energy, neutrinos from DM decay are produced predominantly at an energy of $E_\nu \sim m_{DM}/2$, where m_{DM} is the mass of the DM particle, whereas the spectrum of non-DM neutrinos is expected to be relatively extended in energy. Regarding direction, the flux of neutrinos from DM decay should peak towards the Galactic Center (GC), where DM is concentrated, whereas the diffuse flux of non-DM neutrinos is expected to be isotropic. The above features are essential and generic to UHE neutrinos of DM and non-DM origin alike, and are broadly present in models of their fluxes. By relying on them, our methods apply broadly, regardless of the specific nature of the DM particle, of the relative size of the fluxes of neutrinos from DM decay and of non-DM neutrinos, and of the specific shape of the energy spectrum of non-DM neutrinos.

Our strategy is similar to studies of the decay of TeV–PeV DM that use IceCube data (see, e.g., Ref. [49]), but has one important advantage. In the TeV–PeV range, it is possible

that non-DM astrophysical processes produce an excess of neutrinos towards the GC that could obfuscate a signal of neutrinos from DM decay [75–88]. In contrast, in the UHE range, we expect no astrophysical process to produce neutrinos towards the GC, making the search for DM decay cleaner.

We gear our forecasts to the radio detection of UHE neutrinos in IceCube-Gen2, since it is among the largest upcoming neutrino telescopes under consideration and is presently in an advanced stage of planning. We model neutrino detection via the same state-of-the-art simulations used in Refs. [74,89,90], which account for UHE neutrino propagation inside Earth, detector geometry, energy- and direction-dependent detector response, and energy and angular detector resolution.

Figure 1 summarizes our main findings; we defer details to later. They are twofold: on the discovery of DM decay and on lower limits on the DM lifetime. For the first time, we report robust discovery prospects for UHE neutrinos from DM decay, i.e., the values of DM mass and lifetime that would allow us not only to detect UHE neutrinos, but also to claim that they originate from DM decay, at least partially. In Fig. 1, the presence of about 30 neutrinos from DM decay in a 10-year event sample, would allow us to claim their DM origin. Separately, we find that while the background of non-DM UHE neutrinos weakens the lower limits on DM lifetime, an energy and angular analysis mitigates this weakening, keeping the limits competitive with present-day ones, at worst.

The overarching message of our results is that, despite our ignorance of the background of astrophysical and cosmogenic UHE neutrinos, the discovery of UHE neutrinos will constitute a sensitive probe of heavy DM decay. We present our results and methods to inform future forecasts and searches.

This paper is structured as follows. In Sec. II we discuss the main features of DM and non-DM neutrino production, and highlight the models that we choose as benchmark for this work. In Sec. III we describe how we compute UHE neutrino-induced event rates at IceCube-Gen2. In Sec. IV we obtain the prospects of IceCube-Gen2 for the discovery of DM neutrinos. In Sec. V we forecast bounds on the DM lifetime if no evidence for DM decay is found. In Sec. VI, we conclude. In Appendix, we provide additional figures which complement the results in the main text.

II. FLUXES OF UHE NEUTRINOS

The diffuse flux of UHE astrophysical and cosmogenic neutrinos, itself a target of discovery [64,65,70,74], could be a background to searches for the diffuse flux of UHE neutrinos from DM decay. Fortunately, these fluxes differ in their distributions in energy and direction. In energy, the non-DM background neutrino flux is spread out, while that of neutrinos from DM decay is more concentrated. In direction, the non-DM background neutrino flux is
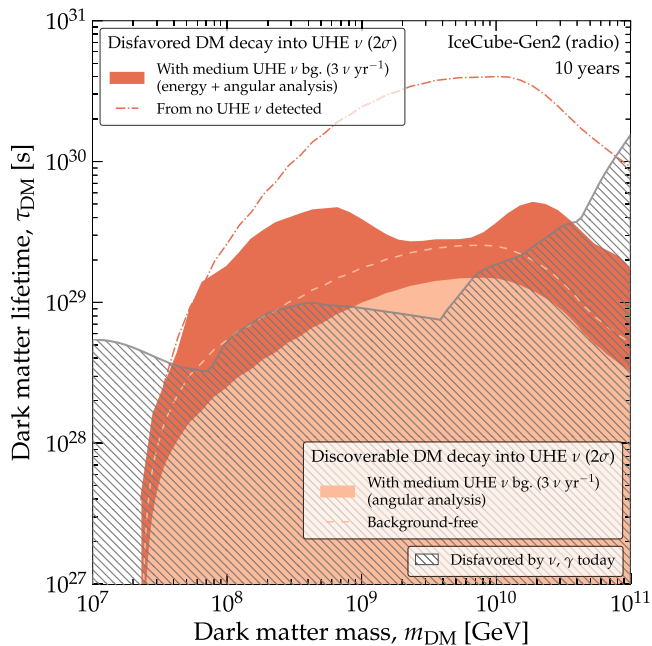
FIG. 1.   Forecasts of discovery and constraints of dark matter decay into UHE neutrinos in the radio array of IceCube-Gen2. DM decay can be discovered or constrained even in the presence of a medium-sized non-DM cosmogenic background flux of UHE neutrinos (Fig. 2). Forecasts are based on state-of-the-art projected samples of detected events with energies over 10^7 GeV, use baseline choices of the detector angular and (logarithmic) energy resolution, $\sigma_\Omega = 3°$ and $\sigma_\epsilon = 0.1$, and assume no knowledge of the non-DM neutrino background in the analysis of projected data. For discovery, forecasts use the angular distribution of events; for constraints, their joint angular and energy distribution. This figure assumes the Navarro-Frenk-White density profile for Galactic DM. Existing lower limits on the DM lifetime are from the upper bound on the UHE neutrino flux from IceCube [91], KASCADE-Grande [92], the Telescope Array [93], and the Pierre Auger Observatory [94]; see Ref. [48]. See Sec. IV for details on discovery (especially Figs. 7–10) and Sec. V for details on bounds (especially Figs. 11 and 12).

isotropic, while that of neutrinos from DM decay peaks towards the Galactic Center. We review these features below; later (Secs. IV and V), we use them to distinguish between the fluxes.

A. UHE astrophysical and cosmogenic neutrinos

UHE neutrinos are expected from the interaction of UHECR protons, with energies $E_p \gtrsim 100$ PeV, with ambient matter [95–97] or radiation [96,98,99], inside the extragalactic astrophysical sources where they are accelerated—i.e., *astrophysical* neutrinos—or with cosmic photon backgrounds during their propagation in extragalactic space—i.e., *cosmogenic* neutrinos. These interactions produce high-energy pions, and other intermediate particles, that promptly decay into high-energy neutrinos via $\pi^- \to \mu^- + \bar{\nu}_\mu$, followed by $\mu^- \to e^- + \bar{\nu}_e + \nu_\mu$, and their

charge-conjugated processes, where each neutrino has energy $E_\nu \simeq E_p/20$.

We focus on the diffuse UHE neutrino flux, i.e., the sum of the UHE neutrino emission—astrophysical or cosmogenic—from all sources, across all redshifts. The cosmogenic neutrino flux is isotropic, since extragalactic magnetic fields scramble the trajectories of neutrino-producing UHECRs; see Sec. II C. The angular distribution of the astrophysical neutrino flux reflects that of the neutrino sources in the sky. Because UHE neutrino sources are in all likelihood extragalactic, we assume that they are isotropically distributed, and so the diffuse neutrino flux from them is isotropic, too. The discovery of the diffuse flux of astrophysical and cosmogenic neutrinos is one of the main goals of the next generation of neutrino telescopes [64,65,74,89]. (The associated discovery of point sources of UHE neutrinos is explored in Refs. [90,100,101].) Yet, in our work, they represent a background to the discovery of neutrinos from DM decay.

Cosmogenic neutrinos were first proposed in the late 1960s [53], as a natural consequence of the interaction of UHECRs on the CMB [72,73]. They constitute a nearly guaranteed contribution in the UHE neutrino range, since their production only relies on the existence of UHECRs and of the CMB (and also of the extragalactic background light). The flux of cosmogenic neutrinos depends on the properties of UHECRs—their spectrum, maximum energies, and mass composition—and of their sources—their distribution in redshift. Because these properties are known uncertainly [102], the flux predictions vary widely, in size and shape; see, e.g., Refs. [31,103–116].

Astrophysical UHE neutrinos are produced inside astrophysical sources. In this case, the target photons need not be the CMB, but low-energy photons present in the environments in which UHECRs are injected. Flux predictions are made more complex because they depend also on the physical conditions inside the sources, including the shape of the photon spectra, the matter density, and the geometry of the neutrino production region. Numerous models have been proposed for various candidate source classes, including active galactic nuclei [109,115,117–126], gamma-ray bursts [127–134], newborn pulsars [108,135], and tidal disruption events [136–144]. In some models, the diffuse astrophysical neutrino flux can be comparable or larger than the cosmogenic neutrino flux; e.g., Ref. [115].

Thus, there is a large number of competing theoretical predictions of the cosmogenic and astrophysical UHE neutrino flux; see Fig. 2 in Ref. [74] and Fig. 6 in Ref. [89] for an overview. The range of predicted UHE neutrino fluxes spans several orders of magnitude. The highest flux predictions [103] would yield about 30 events per year in the radio array of IceCube-Gen2, making them easily discoverable; the lowest [113,115], less than one event in 10 years, making them undiscoverable (see Fig. 1 and Table I in Ref. [74] for details).
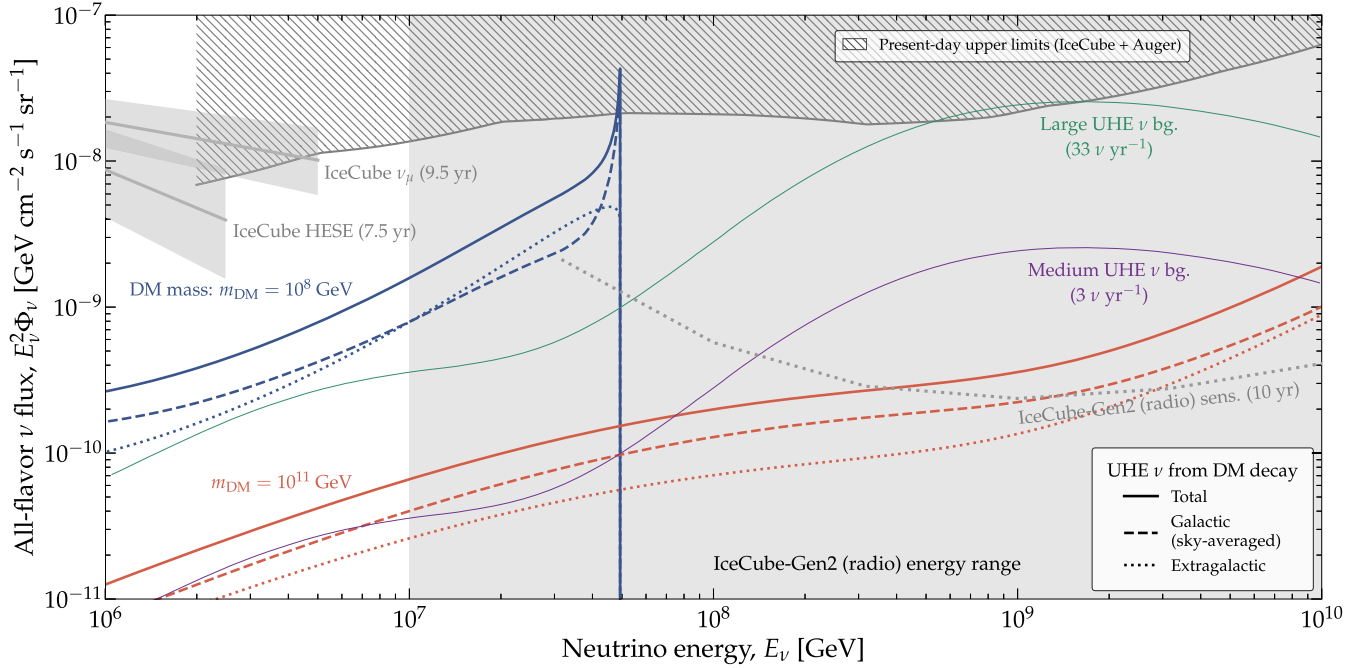
FIG. 2. Diffuse flux of UHE neutrinos from DM decay and non-DM background flux. The flux from the decay of a DM particle, χ, into neutrinos (i.e., $\chi \to \nu + \bar{\nu}$) is shown for illustrative choices of the DM mass, $m_{DM} = 10^8$ GeV and 10^{11} GeV, and of the DM lifetime, $\tau = 10^{29}$ s, and computed following Sec. II B. Later, we vary the values of the DM mass and lifetime in our forecasts. The neutrino flux from DM decay is separated into its sky-averaged Galactic component and its isotropic extragalactic component. (We do not show in this figure the primary-neutrino contribution to the Galactic component, since it is a singular monochromatic line at $E_\nu = m_{DM}/2$, but we include it in our calculations; see Sec. II B.) The two non-DM isotropic UHE neutrino fluxes are the benchmarks that we use in our work. The large benchmark flux is the cosmogenic neutrino flux predicted by Bergman & van Vliet [103] based on cosmic-ray data from the Telescope Array [145,146]. The medium benchmark flux is 10% of that. The projected sensitivity of the radio array of IceCube-Gen2 is from Ref. [149]. Present-day upper limits on the flux of UHE neutrinos are from IceCube [91] and the Pierre Auger Observatory [147]. For comparison, we show the tail end of the present-day IceCube measurements of TeV–PeV neutrinos [31,104]. See Sec. II for details.

Most flux predictions share some common features; e.g., they can be roughly described as a power-law flux—from neutrino production via proton-matter interactions—a bumplike flux—from neutrino production via proton-photon interactions—or a combination of both. The resemblance between different flux predictions is largely superficial, since they differ in a number of important assumptions, i.e., the identity of the neutrino sources, the physical conditions in the region of neutrino production, the neutrino production mechanism, and the UHECR observations on which the neutrino predictions are based. Regardless, in our forecasts below, we pivot on these superficial similarities and choose a benchmark background flux of UHE neutrinos that is representative of the range of theoretical predictions.

Figure 2 shows the two illustrative flux predictions that we select as benchmark "non-DM" UHE neutrino background for our analysis. They represent a large background and an intermediate one; later, we complement them with a null-background scenario. We base both on the cosmogenic neutrino flux predicted by Bergman & van Vliet [103] by fitting the simulated UHECR energy spectrum and mass

composition at Earth to recent data from the Telescope Array (TA) [145,146]. (This is flux model 4 in Refs. [74,89].) Because TA data favors a light UHECR mass composition and high maximum rigidity, the resulting cosmogenic neutrino flux is large: Fig. 2 shows that it saturates the present-day upper limits from IceCube [91] and the Pierre Auger Observatory [147].

Large non-DM background: This is the full cosmogenic neutrino flux predicted by Bergman & van Vliet [103], which yields about 33 events per year in the radio array of IceCube-Gen2; see Figs. 3 and 4 and Table I in Ref. [74], and Fig. 5 below. Because this is as large a flux of UHE neutrinos as is allowed by present-day upper limits (Fig. 2), it is about the largest background of non-DM UHE neutrinos that we could face in a search for DM decay.

Intermediate non-DM background: This is the Bergman & van Vliet cosmogenic flux scaled down to 10% of its size, which yields about three events per year in the radio array of IceCube-Gen2.

Null background: The ideal scenario for the discovery of UHE neutrinos from DM is the absence of non-DM

UHE neutrinos. This has been the scenario adopted in previous forecasts of DM decay into UHE neutrinos [71,148]. We maintain it here as a baseline against which we compare our forecasts including a non-DM background.

Figure 2 shows the all-flavor background flux, but when computing event rates (Sec. III) we sum the individual contributions of the fluxes of ν_e, $\bar{\nu}_e$, ν_μ, $\bar{\nu}_\mu$, ν_τ, and $\bar{\nu}_\tau$ for this model, as shown in Fig. 6 in Ref. [89].

For the purpose of discovering neutrinos from DM decay, what matters is not whether the non-DM UHE neutrino background is cosmogenic or astrophysical, but rather that its angular and energy distributions are different from those of the flux of neutrinos from DM decay (Sec. I). We point out these differences explicitly in Sec. II C. Admittedly, in choosing a benchmark non-DM UHE neutrino background, we make a specific choice of the shape of its energy spectrum. This choice is necessary to be able to generate simulated samples of detected events (Sec. III). However, when analyzing these samples (Secs. V and IV), we do not assume knowledge of the size or shape of the non-DM background, but instead let them vary, just as an analysis of real detected data would.

B. UHE neutrinos from dark matter decay

The decay of a heavy DM particle, χ, with mass $m_{\mathrm{DM}} \gtrsim 10^7$ GeV, into Standard Model particles, leads to the production of high-energy neutrinos. The yield of neutrinos depends on the channels by which the DM particle decays. If the DM particle decays primarily into neutrinos, i.e., $\chi \to \bar{\nu}\nu$, then the resulting neutrino flux has a primary contribution that is monoenergetic at $E_\nu = m_{\mathrm{DM}}/2$. We neglect the spread of the energy spectrum due to the thermal velocity of DM, since it is small [150,151]. A secondary contribution comes from electroweak corrections, generated from the emission, by the decay products, of off-shell W and Z bosons that promptly decay into neutrinos; this contribution is present even if DM does not primarily decay to neutrinos. In our analysis, we consider the neutrino flux made up of both primary and secondary contributions.

The electroweak corrections unavoidably give rise to gamma rays, electrons, positrons, protons, and antiprotons that are also amenable to indirect detection. Upper limits on their flux indirectly constrain the associated neutrino flux. Notably, for most decay channels (e.g., for hadronic decay channels such as $\chi \to b\bar{b}$), the present-day upper limits on the gamma-ray flux are so strong that the projected limits on the associated UHE neutrino flux are comparable or weaker; see, e.g., Ref. [148] (see also Ref. [152] for a comparison of the bounds from gamma-ray and cosmic-ray measurements). However, for leptonic (e.g., $\chi \to \bar{\tau}\tau$) and neutrinophilic (i.e., $\chi \to \bar{\nu}\nu$) decay channels, in the DM mass range $m_{\mathrm{DM}} = 10^7$–10^{10} GeV, the bounds from UHE neutrinos may be comparable or stronger than the

present-day bounds from gamma rays. For this reason, we focus exclusively on the neutrinophilic decay channel, $\chi \to \bar{\nu}\nu$. We assume equal branching ratios for the decay into each of the three flavors, $\chi \to \bar{\nu}_e\nu_e$, $\chi \to \bar{\nu}_\mu\nu_\mu$, and $\chi \to \bar{\nu}_\tau\nu_\tau$. We treat the flux of ν_e, $\bar{\nu}_e$, ν_μ, $\bar{\nu}_\mu$, ν_τ, and $\bar{\nu}_\tau$ separately; later, we propagate each through the Earth (Sec. III A) and compute its contribution to the detected event rate (Sec. III B).

We compute the neutrino spectra numerically, using the public code HDMSpectra [153], which evolves the particle showers initiated by DM decay, including in detail electroweak corrections, and yields the final-state products of shower evolution. The neutrino spectra from DM decay are notoriously hard to compute precisely, since the emission of soft collinear $W^\pm$ bosons leads to logarithmically enhanced terms $\propto \log^2(m_{\mathrm{DM}}/m_W)$, where m_W is the mass of the W boson, that need to be resummed [154]; HDMSpectra accounts for this. Thus, from HDMSpectra we obtain dN_{ν_α}/dE_ν and $dN_{\bar{\nu}_\alpha}/dE_\nu$ ($\alpha = e, \mu, \tau$), the number of ν_α and $\bar{\nu}_\alpha$ emitted in a single DM decay per unit energy. These spectra include also the primary monoenergetic contributions at $E_\nu = m_{\mathrm{DM}}/2$.

The diffuse flux of neutrinos that reach the Earth is due to DM decays that occur inside the Galaxy (Gal) and in extragalactic space (EG), i.e.,

$$\frac{d\Phi_{\nu_\alpha}}{dE_\nu d\Omega_\nu} = \frac{d\Phi_{\nu_\alpha}^{\mathrm{Gal}}}{dE_\nu d\Omega_\nu} + \frac{d\Phi_{\nu_\alpha}^{\mathrm{EG}}}{dE_\nu d\Omega_\nu}, \qquad (1)$$

where Ω_ν is the solid angle. To compute the Galactic contribution, we integrate the neutrino spectrum from a single DM decay over the spatial distribution of DM in the Milky Way. This makes the Galactic neutrino flux anisotropic, since it traces the density of Galactic DM. To compute the extragalactic contribution, we integrate the neutrino spectrum from a single DM decay over the cosmological distribution of DM. This makes the extragalactic neutrino flux isotropic.

The Galactic contribution of ν_α is

$$\frac{d\Phi_{\nu_\alpha}^{\mathrm{Gal}}}{dE_\nu d\Omega_\nu} = \frac{dN_{\nu_\alpha}}{dE_\nu} \int_0^\infty \frac{\rho_{\mathrm{DM}}(s,b,l)}{4\pi\tau_{\mathrm{DM}} m_{\mathrm{DM}}} ds, \qquad (2)$$

where s is the distance measured from the Earth, b and l are Galactic latitude and longitude and parametrize the neutrino incoming direction, τ_{DM} is the DM lifetime, and ρ_{DM} is the density profile of DM in the Galaxy.

Figure 3 shows competing models of the Galactic DM density profiles. The "cuspy" Navarro-Frenk-White (NFW) [155] profile—obtained from a numerical fit to N-body simulations of structure formation—and Einasto [156] profile—originally proposed to describe stellar systems and later extended to fit the DM halo—peak towards the GC. The "puffy" Burkert profile [157]—obtained by a fit to the DM distribution in dwarf galaxies—instead plateaus to
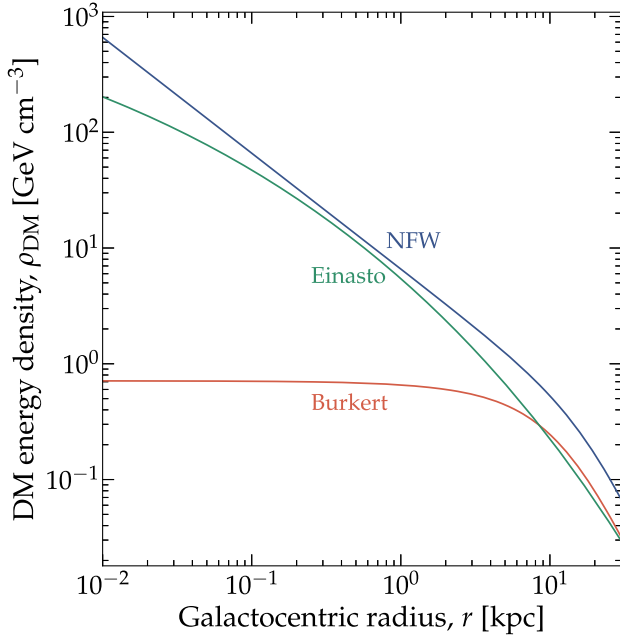
FIG. 3.   Profiles of Galactic dark matter density. For the Navarro-Frenk-White (NFW) profile [155], we use Eq. (3). For the Einasto [156] and Burkert [157] profiles, we use the parametrizations and parameter choices from Ref. [158]; see Eq. (4). Our main results for DM discovery (Figs. 7, 9, 10, and 14) and bounds (Figs. 11, 12, and 15) are generated assuming the NFW profile. Results generated assuming the Einasto profile (not shown) are similar. Figures 8 and 13 contrast results obtained assuming the NFW and Burkert profiles.

a core towards the GC. We pick the NFW and Burkert profiles as representative of the two extremes of the "cusp vs core" uncertainty in Galactic DM profiles. To produce our main results, in Figs. 7, 9, 10, 11, 12, 14, and 15, we adopt the NFW profile; in Figs. 11, 12, and 15, we contrast them against results obtained assuming the Burkert profile. For the NFW profile, we use [158]

$$\rho_{\rm DM}^{\rm NFW}(s, b, l) = \frac{\rho_0}{\left(\frac{r(s,b,l)}{r_c}\right)\left(1 + \frac{r(s,b,l)^2}{r_c^2}\right)}, \qquad (3)$$

where $\rho_0 = 0.33$ GeV cm^{-3}, $r_c = 20$ kpc, and $r(s, b, l) = \sqrt{s^2 + R_s^2 - 2sR_s \cos b \cos l}$ is the Galactocentric radius, with $R_s = 8.5$ kpc. For the Burkert profile, we use

$$\rho_{\rm DM}^{\rm Burkert}(s, b, l) = \frac{\rho_s}{\left(1 + \frac{r(s,b,l)}{r_s}\right)\left(1 + \frac{r(s,b,l)^2}{r_s^2}\right)}, \qquad (4)$$

with $\rho_s = 0.712$ GeV cm^{-3} and $r_s = 12.67$ kpc [158].
   The extragalactic contribution of ν_α is

$$\frac{d\Phi_{\nu_\alpha}^{\rm EG}}{dE_\nu d\Omega_\nu} = \frac{\Omega_{\rm DM}\rho_c}{4\pi\tau_{\rm DM}m_{\rm DM}} \int_0^\infty \frac{dz}{H(z)} \left. \frac{dN_{\nu_\alpha}}{dE_\nu} \right|_{E_\nu(1+z)}, \qquad (5)$$

where z is the redshift, $\rho_c = 4.79 \times 10^{-6}$ GeV cm^{-3} is the critical density of the Universe, $\Omega_{\rm DM} = 0.265$ is the fraction of energy density of the Universe in the form of DM, $H(z) = H_0\sqrt{\Omega_\Lambda + \Omega_m(1+z)^3}$ is the Hubble parameter, $H_0 = 1.08 \times 10^{-28}$ cm^{-1} h is the Hubble constant, with $h = 0.674$, $\Omega_\Lambda = 0.685$ is the vacuum energy density, and $\Omega_m = 0.315$ is the matter energy density. The right-hand side of Eq. (5) is evaluated at an energy $E_\nu(1+z)$ to compensate for the cosmological expansion.
   Figure 2 shows the resulting diffuse energy spectrum of UHE neutrinos from DM decay, integrated over all sky directions, for two benchmark values of the DM mass, and separated into the Galactic and extragalactic components only for illustration. The main features of the energy spectrum are a spike of neutrinos close to the energy $E_\nu = m_{\rm DM}/2$, and a power-law tail at lower energies, from electroweak corrections and, in the case of the extragalactic component, from redshifting. The dominant component of the flux is the Galactic one, due to the nearby DM overdensity in the GC. However, at energies close to the spike, a pileup of neutrinos from the direct decay $\chi \to \bar\nu\nu$, redshifted to lower energies, causes the extragalactic contribution to dominate instead in a narrow energy range. Because we assume DM decay into neutrinos of all flavors with equal branching ratios (see above), the all-flavor flux in Fig. 2 is split evenly among the three flavors and among neutrinos and antineutrinos.

C. Non-DM neutrinos vs neutrinos from DM decay

   The essential differences between the background flux of UHE non-DM neutrinos and the flux of UHE neutrinos from DM decay are in their energy spectrum and in their angular distribution in the sky.
Energy spectrum: Figure 2 shows that the energy spectrum of our benchmark non-DM background flux—which is typical of many flux predictions—is more spread out around its maximum compared to the energy spectrum of neutrinos from DM decay, which peaks sharply at $E_\nu = m_{\rm DM}/2$. Yet, because of the spread of the latter towards lower energies due to redshifting (compounded, later, by the limited energy resolution of the detector), the differences in spectral shape are not as marked. While the lack of a bumplike feature in the observed spectrum of UHE neutrinos would disfavor DM decay, its observation could be attributed either to DM decay or to a non-DM background flux. Accordingly, the energy spectrum is not the driving factor to discover DM decay (Sec. IV), but supplements angular information to set constraints (Sec. V).
Angular distribution: Figure 4 shows the angular distribution of the total diffuse flux of UHE neutrinos, integrated over energy. This reveals the critical difference between non-DM and DM neutrinos: the flux of non-DM neutrinos is isotropic, while the flux of DM neutrinos peaks towards the GC, where, under the NFW profile, it is about a factor
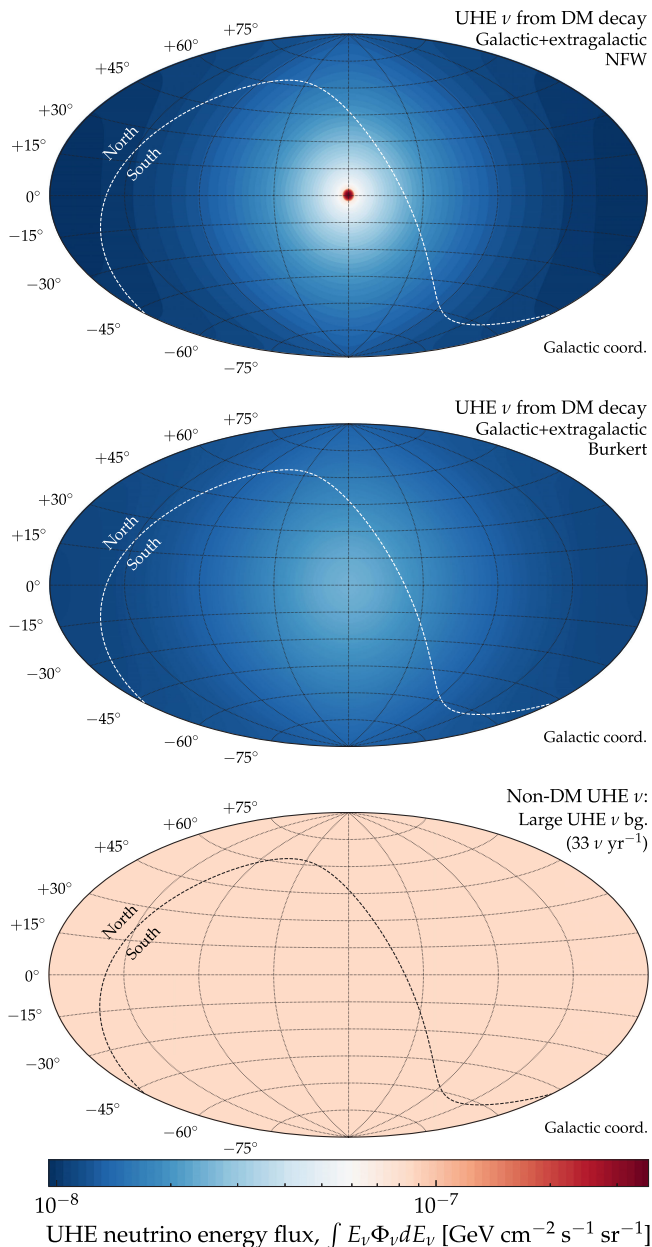
FIG. 4. Angular distribution of the diffuse flux of UHE neutrinos. Top: neutrinos from DM decay, for a NFW profile. We show the distribution computed using illustrative values of DM mass and lifetime, $m_{\rm DM} = 10^8$ GeV and $\tau_{\rm DM} = 10^{29}$ s, but for other values the angular distribution is very similar. Center: same for a Burkert profile. Bottom: neutrinos from the non-DM isotropic background of UHE neutrinos. The flux is isotropic, so the sky map is shaded uniformly. We show the distribution from our large benchmark background, i.e., the cosmogenic neutrino flux by Bergman & van Vliet [103], but for other choices of the isotropic background flux the angular distribution is very similar.

20 larger than in the rest of the sky. This contrast is the main driving factor to discover DM decay and place constraints on it. For the puffier Burkert profile, the contrast is milder, which weakens both prospects, as we show later. In either

case, because the GC is in the Southern Hemisphere, neutrinos from DM decay coming from this direction are not attenuated by their passage through Earth before reaching IceCube-Gen2 (Sec. III A), making it particularly sensitive to this signal.

Below (Sec. III), we show that the above differences between the fluxes are mirrored, albeit imperfectly, by corresponding differences in the energy and angular distributions of detected events.

III. DETECTION OF UHE NEUTRINOS

To make realistic forecasts of probes of DM decay into UHE neutrinos, we compute in detail their propagation inside the Earth and their radio detection in our detector of choice, the radio array of IceCube-Gen2.

A. Neutrino propagation inside the Earth

Upon reaching Earth, UHE neutrinos propagate from its surface, through its interior, to the detector, IceCube-Gen2, situated at the South Pole. While propagating, neutrinos interact with matter underground. Because the neutrino-nucleon cross section, $\sigma_{\nu N}$, grows with neutrino energy (at ultrahigh energies, roughly as $\sigma_{\nu N} \propto E_\nu^{0.363}$ [159]), these interactions appreciably attenuate the flux of neutrinos that reaches the detector. Roughly, neutrino interactions attenuate the flux via an exponential dampening factor $e^{-\sigma_{\nu N} L}$, where L is the distance traveled underground. Thus, the attenuation grows with neutrino energy and with distance traveled.

At ultrahigh energies, neutrinos interact with nucleons predominantly via deep inelastic scattering (DIS) [160–166]. In it, the incoming neutrino scatters off of a parton—a quark or a gluon—of a nucleon at rest, N—a proton or a neutron ($N = p, n$). The interaction is neutral-current (NC) if mediated by a Z boson, i.e., $\nu_\alpha + N \to \nu_\alpha + X$ ($\alpha = e, \mu, \tau$), where X represents final-state hadrons, or charged-current (CC) if mediated by a W boson, i.e., $\nu_\alpha + N \to \alpha + X$. The NC neutrino-nucleon cross section, $\sigma_{\nu_\alpha N}^{\rm NC}$, is about 1/3 of the CC cross section, $\sigma_{\nu_\alpha N}^{\rm CC}$. At these energies, the cross sections on proton and on neutron are very similar, and the cross sections for different neutrino flavors are nearly equal. When propagating neutrinos inside the Earth, and also when computing detected event rates (Sec. III C), we treat separately the NC and CC interactions of neutrinos of different flavors, each with its own cross section.

In a DIS interaction, the final-state hadrons receive a fraction y—the inelasticity—of the energy of the interacting neutrino. The final-state leptons receive the remaining fraction, $(1 - y)$. The inelasticity follows a probability distribution given by the differential cross sections, either $d\sigma_{\nu_\alpha N}^{\rm NC}/dy$ or $d\sigma_{\nu_\alpha N}^{\rm CC}/dy$. The distributions peak at $y = 0$, but they are broad, and depend on the neutrino energy; see, e.g., Fig. 4 in Ref. [89].

Thus, as neutrinos propagate inside the Earth, NC interactions shift the neutrino flux to lower energies, while CC interactions deplete the flux. (For ν_τ, the consecutive CC neutrino interactions and decays of the ensuing tauons—known as "ν_τ regeneration"—appreciably counteract the flux dampening; see, e.g., Fig. 8 in Ref. [89].) At ultrahigh energies, the flux of up-going neutrinos, with $\theta_z > 90°$, where θ_z is the zenith angle measured from the South Pole, is nearly fully attenuated by the time it reaches the detector. On the contrary, the flux of down-going ($\theta_z < 90°$) and horizontal ($\theta_z \approx 90°$) neutrinos is attenuated appreciably, but is not completely depleted. For illustration, see, e.g., Fig. A2 in Ref. [164], Ref. [167], and Figs. 10 & 11 in Ref. [89]. This makes the detection of UHE neutrinos more likely from these directions, provided there is sufficient detector response, which is the case for our modeling of IceCube-Gen2; we elaborate on this in Secs. III B and III C.

We compute the propagation of UHE neutrinos inside the Earth as in Refs. [74,89,90], using the sophisticated propagation code NUPROPEARTH [167,168]. It uses the recent BGR18 neutrino-nucleon DIS cross sections [13], the same ones that we use in Sec. III C to compute the rate of detected events. NUPROPEARTH also accounts for ν_τ regeneration, for energy losses of intermediate leptons during propagation, and for subleading neutrino interactions that, taken together, increase the flux attenuation by approximately an extra 10%. For the density profile of matter inside the Earth, we adopt the Preliminary Reference Earth Model [169], with an added layer of surface ice 3 km thick to represent Antarctica, and account also for the radial change in the chemical composition of underground matter [167]. Finally, we model the volume of the neutrino detector—the radio array of IceCube-Gen2—as a cylinder of radius 12.6 km and height 1.50 km, buried vertically 100 m underground at the South Pole; see Fig. 7 in Ref. [89].

In summary, given a flux of neutrinos at the surface of the Earth, from DM decay or from the non-DM background neutrino flux, we propagate it across many different directions to the detector. We propagate separately the fluxes of ν_e, $\bar{\nu}_e$, ν_μ, $\bar{\nu}_\mu$, ν_τ, and $\bar{\nu}_\tau$;. Below, we use their fluxes at the detector, $\Phi^{\text{det}}_{\nu_\alpha}$ and $\Phi^{\text{det}}_{\bar{\nu}_\alpha}$, to compute neutrino-induced event rates.

B. UHE neutrino radio detection at IceCube-Gen2

Reference [170] first proposed using the radio emission from UHE particles as a means to detect them. Upon reaching the detector volume, an UHE neutrino may scatter off a nucleon in ice and produce a shower of high-energy particles. As the shower travels, it accumulates an excess of electrons in its front that, after reaching shower maximum, is emitted as an impulsive coherent radio pulse, known as Askaryan radiation [171]. For details, see Refs. [172,173]. Because radio travels in ice subject only to mild

attenuation, it may be detected using a sparse underground array of radio antennas, which makes it feasible to instrument a large volume that makes up for the potentially tiny fluxes of incoming UHE neutrinos.

This is the strategy adopted by the planned radio array of IceCube-Gen2 [63]. Of the proposed UHE neutrino telescopes [65,70,174], the radio array of IceCube-Gen2 is among the largest and in an advanced stage of planning [63]. Thus, we gear our forecasts to it. However, our methods can be readily adapted to other upcoming UHE neutrino telescopes [65,70,174].

To compute realistic projected event rates at the radio array of IceCube-Gen2, we follow the detailed procedure introduced in Ref. [89], which uses an estimated detector response based on state-of-the-art simulations. This has been used already to forecast the measurement of the UHE neutrino-nucleon cross section [89], the discovery of UHE neutrino point sources [90], and the discovery of the diffuse flux of UHE neutrinos [74]. Below, we only sketch the procedure and introduce necessary modifications to it; we defer to Ref. [89] for details.

Upon reaching the detector volume, after propagating through the Earth (Sec. III A), an UHE ν_α of energy E_ν interacts with a nucleon at rest, N, typically via DIS (see above). The ensuing particle shower has an energy E_{sh}, a fraction of the parent neutrino energy. For showers initiated by the NC DIS of ν_α or $\bar{\nu}_\alpha$ of any flavor, only the final-state hadrons radiate [175], so $E_{\text{sh}} = yE_\nu$. For showers initiated by the CC DIS of a ν_e or $\bar{\nu}_e$, both the final-state electron and hadrons radiate, so $E_{\text{sh}} = E_\nu$. For showers initiated by the CC DIS of ν_μ, $\bar{\nu}_\mu$, ν_τ, or $\bar{\nu}_\tau$, only the final-state hadrons radiate, so $E_{\text{sh}} = yE_\nu$. As during propagation, at detection the value of the inelasticity follows $d\sigma^{\text{NC}}_{\nu_\alpha}/dy$ and $d\sigma^{\text{CC}}_{\nu_\alpha}/dy$, for which we adopt the BGR18 [13] calculation; see Fig. 4 in Ref. [89].

The detector response is represented by its effective volume, which we treat separately for NC and CC showers, $V^{\text{NC}}_{\text{eff},\nu_\alpha}$ and $V^{\text{CC}}_{\text{eff},\nu_\alpha}$. The effective volume depends on the shower energy and on the direction of the incoming neutrino. It is generated by simulating the interaction of neutrinos in the detector volume, followed by the generation of Askaryan radiation, its propagation in ice, including changes in the index of refraction of ice with depth, and its detection in the two types of radio antennas envisioned in the array. For the simulations we use NURADIORECO [176] and NURADIOMC [177], the same tools used by the IceCube-Gen2 Collaboration. We adopt the same array design consisting of a combination of shallow and deep radio stations as in Ref. [89]. The effective volume is least sensitive around 10^7 GeV, grows with shower energy, and is relatively less sensitive for down-going neutrinos ($\cos\theta_z \approx 1$); see Fig. 13 in Ref. [89]. (Unlike common practice, the detector volume does not contain the effect of the attenuation of the neutrino flux underground. This is contained separately in $\Phi^{\text{det}}_{\nu_\alpha}$.)

The differential event rate is obtained by convolving the neutrino flux that reaches the detector (Sec. III A), $\Phi_{\nu_\alpha}^{\mathrm{det}}$, the effective volume, and the neutrino-nucleon cross section. For ν_α, after an exposure time T, this is

$$\frac{d^2N_{\nu_\alpha}}{dE_{\mathrm{sh}}d\cos\theta_z d\phi} = Tn_t \int_0^1 dy \left(\frac{E_{\nu_\alpha}^{\mathrm{NC}}(E_{\mathrm{sh}},y)}{E_{\mathrm{sh}}} V_{\mathrm{eff},\nu_\alpha}^{\mathrm{NC}}(E_{\mathrm{sh}},\cos\theta_z) \frac{d\sigma_{\nu_\alpha\mathrm{w}}^{\mathrm{NC}}(E_\nu,y)}{dy} \Phi_{\nu_\alpha}^{\mathrm{det}}(E_\nu,\cos\theta_z,\phi) \Big|_{E_\nu = E_{\nu_\alpha}^{\mathrm{NC}}(E_{\mathrm{sh}},y)} + \mathrm{NC}\to\mathrm{CC} \right), \quad (6)$$

where $d\sigma_{\nu_\alpha\mathrm{w}}^{\mathrm{NC}}/dy$ is the cross section for interaction with water, made up of ten protons and eight neutrons, and n_t is the number density of water molecules in ice. The event rate due to $\bar{\nu}_\alpha$ is the same as Eq. (6), but changing $\Phi_{\nu_\alpha}^{\mathrm{det}} \to \Phi_{\bar{\nu}_\alpha}^{\mathrm{det}}$, $d\sigma_{\nu_\alpha}^{\mathrm{NC}}/dy \to d\sigma_{\bar{\nu}_\alpha}^{\mathrm{NC}}/dy$, and $d\sigma_{\nu_\alpha}^{\mathrm{NC}}/dy \to d\sigma_{\bar{\nu}_\alpha}^{\mathrm{CC}}/dy$. At these energies the cross sections for ν_α and $\bar{\nu}_\alpha$ are nearly indistinguishable; see Ref. [13] and Fig. 3 in Ref. [89]. Equation (6) generalizes the original procedure in Ref. [89] by allowing the flux and the event rate to vary not only with zenith angle, θ_z, but also with azimuth, ϕ. This allows our analysis to be sensitive to an excess of UHE neutrinos from the decay of DM towards the GC.

As in Ref. [89], we smear the event rate using the detector energy and angular resolution and use for our forecasts the event rate in terms of the reconstructed shower energy, $E_{\mathrm{sh}}^{\mathrm{rec}}$, and reconstructed direction, Ω^{rec}, i.e.,

$$\frac{d^2N_{\nu_\alpha}}{dE_{\mathrm{sh}}^{\mathrm{rec}}d\Omega^{\mathrm{rec}}} = \int dE_{\mathrm{sh}} \int d\Omega \frac{d^2N_{\nu_\alpha}(E_{\mathrm{sh}},\theta_z,\phi)}{dE_{\mathrm{sh}}d\Omega}$$
$$\times R_{E_{\mathrm{sh}}}(E_{\mathrm{sh}}^{\mathrm{rec}},E_{\mathrm{sh}})R_\Omega(\mathbf{n}^{\mathrm{rec}},\mathbf{n}), \quad (7)$$

where $d\Omega = \sin\theta_z d\theta_z d\phi$ and $d\Omega^{\mathrm{rec}} = \sin\theta_z^{\mathrm{rec}} d\theta_z^{\mathrm{rec}} d\phi^{\mathrm{rec}}$ are the real and reconstructed differential solid angles, and $\mathbf{n}$ and $\mathbf{n}^{\mathrm{rec}}$ are the real and reconstructed shower directions. We model the energy resolution via a Gaussian function in $\epsilon \equiv \log_{10}(E_{\mathrm{sh}}^{\mathrm{rec}}/E_{\mathrm{sh}})$, i.e.,

$$R_{E_{\mathrm{sh}}}(E_{\mathrm{sh}}^{\mathrm{rec}},E_{\mathrm{sh}}) = \sqrt{\frac{2}{\pi}} \frac{\exp\left[-\frac{(E_{\mathrm{sh}}^{\mathrm{rec}}-E_{\mathrm{sh}})^2}{2\sigma_{E_{\mathrm{sh}}}^2}\right]}{\sigma_{E_{\mathrm{sh}}}\left[1 + \mathrm{Erf}\left(\frac{E_{\mathrm{sh}}^{\mathrm{rec}}}{\sqrt{2}\sigma_{E_{\mathrm{sh}}}}\right)\right]}, \quad (8)$$

where $\sigma_{E_{\mathrm{sh}}} = 10^{\sigma_\epsilon} E_{\mathrm{sh}}$. As baseline, we fix $\sigma_\epsilon = 0.1$, based on simulations performed for UHE neutrino radio detection at the RNO-G neutrino telescope [178], which we take as representative of IceCube-Gen2, too. We model the angular resolution via a Gaussian function of the angle between true and reconstructed direction, i.e.,

$$R_\Omega(\mathbf{n}^{\mathrm{rec}},\mathbf{n}) = \frac{\sigma^2}{2\pi(1 - e^{-2/\sigma^2})} \exp\left(\frac{\mathbf{n}\cdot\mathbf{n}_{\mathrm{rec}}}{\sigma^2}\right), \quad (9)$$

with a common width of $\sigma_{\theta_z} = \sigma_\phi = \equiv\sigma_\Omega$ in zenith and azimuth. As baseline, we fix $\sigma_\Omega = 3°$, similar to what Ref. [89] adopted for the zenith-angle resolution. References [74,89] explored the effect of varying the energy and angular resolution on the event rate.

To produce our forecasts, we use the all-flavor event rate of ν_α and $\bar{\nu}_\alpha$, i.e.,

$$\frac{d^2N_\nu}{dE_{\mathrm{sh}}^{\mathrm{rec}}d\Omega^{\mathrm{rec}}} = \sum_{\alpha=e,\mu,\tau} \left(\frac{d^2N_{\nu_\alpha}}{dE_{\mathrm{sh}}^{\mathrm{rec}}d\Omega^{\mathrm{rec}}} + \frac{d^2N_{\bar{\nu}_\alpha}}{dE_{\mathrm{sh}}^{\mathrm{rec}}d\Omega^{\mathrm{rec}}} \right). \quad (10)$$

Conservatively, we do not assume that radio detection at IceCube-Gen2 will be able to distinguish between events initiated by different flavors; however, there is promising ongoing work in this direction [175,179,180].

C. Expected event rates

Using the methods above, we compute event rates for the flux of UHE neutrinos from DM decay and for the non-DM background flux of UHE neutrinos. For the former, the event rate depends on the DM mass and lifetime. For the latter, it depends on our choice of background flux. As illustration, below we show event rates for the fluxes in Fig. 2; later, when producing results, we compute event rates for many more cases.

Figure 5 shows the all-sky differential event rate in reconstructed shower energy. The event energy spectra reflect the features of the underlying neutrino energy spectra in Fig. 2, though smoothed out by the detector energy resolution, which complicates distinguishing between them in our forecasts later (see also Sec. II C). Further, while the neutrino energy spectrum from DM decay with $m_{\mathrm{DM}} = 10^8$ GeV and the spectrum of the large non-DM benchmark flux are comparable in Fig. 2; in Fig. 5 the event rate for the former is appreciably smaller than that for the latter. This is because the effective volume falls at low energies, where the spectrum from DM decay peaks; see Sec. III B.

Figure 6 shows sky maps of the angular distribution of the energy-integrated event rate, for neutrinos from DM decay and for the background neutrinos. The angular distribution of events is anisotropic, even when it is due to an isotropic neutrino flux, like the background flux. The radio array of IceCube-Gen2 is mostly sensitive to zenith angles between 45° and 90°. At larger zenith angles, Earth attenuation strongly reduces the chances of neutrino detection, whereas at smaller zenith angles the effective volume is smaller. For this reason, most of the events come from declinations between −45° and 0°. (The two bright zenith bands in the skymaps, easily visible for neutrinos from DM decay, are due to features in the response of the
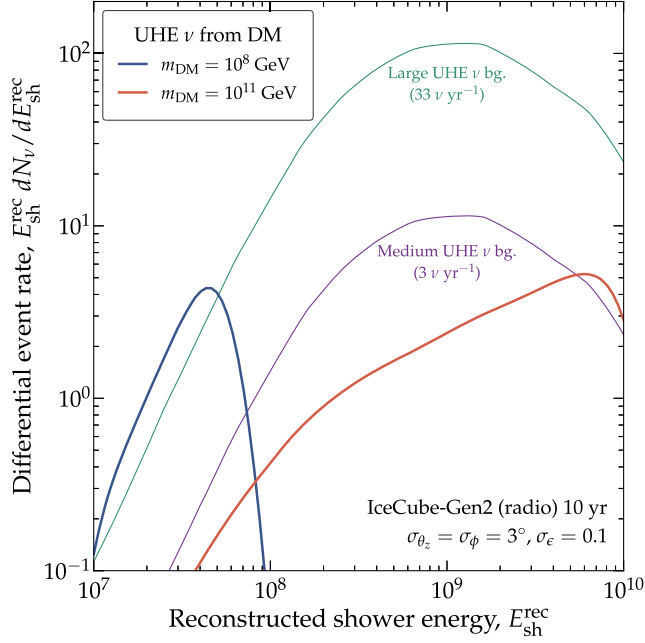
FIG. 5. Differential rate of neutrino-induced events in the radio array of IceCube-Gen2. We show results obtained for the same illustrative choices of the flux from DM decay and the non-DM background flux as in Fig. 2. The event rate is computed using Eq. (10), using baseline choices of the detector angular and (logarithmic) energy resolution, $\sigma_\Omega = 3°$ and $\sigma_\epsilon = 0.1$. This figure shows the direction-averaged energy distribution of events; Fig. 6 shows the angular event distribution. See Sec. III for details.

two types of antennas that the radio array is made of; see Fig. 12 in Ref. [89].)

The sky maps in Fig. 6 illustrate the combined effect of the three sources of angular dependence in our calculation: from the neutrino flux itself, from the propagation of neutrinos through the Earth, and from the detector effective volume. The latter two, together with the angular resolution of the detector, smooth out any natural anisotropy in the neutrino flux. Nevertheless, Fig. 6 shows that the excess of neutrinos from DM decay towards the GC survives into the angular distribution of events, though it is more spread out. The excess is more concentrated for the NFW profile than for the Burkert profile, reflecting their fluxes from Fig. 6.

IV. DISCOVERY PROSPECTS FOR DARK MATTER DECAY

The decay of heavy DM into UHE neutrinos may be discovered even in the presence of sizable non-DM neutrino backgrounds, by using the angular distribution of detected events, in 10 years of exposure of the radio array of IceCube-Gen2 (Fig. 7). However, a puffy Galactic DM density profile may weaken the discovery prospects (Fig. 8). Upon discovery, the DM mass and lifetime, and
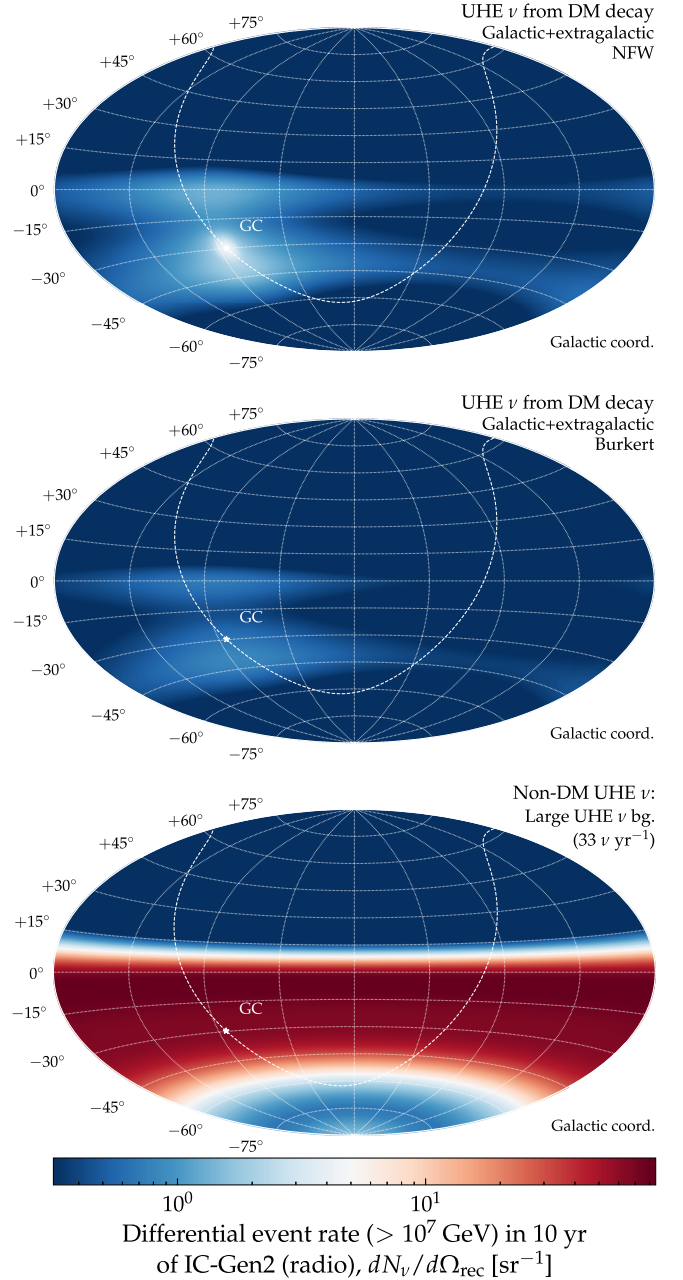

FIG. 6. Angular distribution of detected events in the radio array of IceCube-Gen2. We use the same illustrative fluxes as in Fig. 4. Top: Neutrinos from DM decay for an NFW profile. Center: same for a Burkert profile. Bottom: neutrinos from the non-DM isotropic background of UHE neutrinos. The angular dependence is due both to the angular distribution of the flux (Fig. 4) and the angular response of the detector (Fig. 13 in Ref. [89]). The event rate is computed using Eq. (10), using baseline choices of the detector angular and (logarithmic) energy resolution, $\sigma_\Omega = 3°$ and $\sigma_\epsilon = 0.1$. This figure shows the energy-integrated angular distribution of events; Fig. 5 shows the energy distribution. See Sec. III for details.

the flux of neutrinos from its decay, may be accurately and precisely measured by using also the energy distribution of events (Figs. 9 and 10).
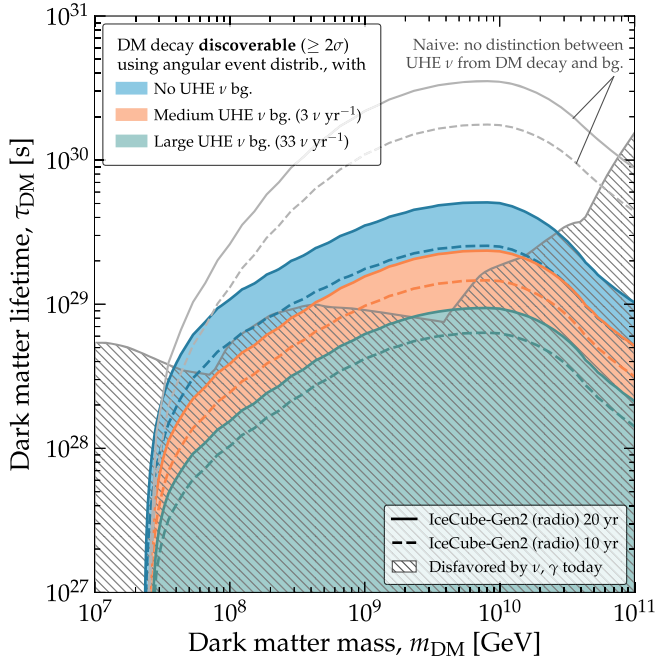
FIG. 7. Discovery prospects of UHE neutrinos from DM decay in the radio array of IceCube-Gen2. Forecasts are for three benchmark choices of the background flux of non-DM UHE neutrinos (i.e., cosmogenic): null, medium, and large (Sec. II A), based on the cosmogenic neutrino flux by Bergman & van Vliet [103] (Fig. 2). The forecasts use only the angular distribution of events, summed over all reconstructed energies $E_{sh}^{rec} \geq 10^7$ GeV. They use baseline choices of the detector angular and (logarithmic) energy resolution, $\sigma_\Omega = 3°$ and $\sigma_\epsilon = 0.1$; see Sec. III B. This figure assumes the NFW density profile for Galactic DM. Existing lower limits on the DM lifetime are the same as in Fig. 1. In this figure, results are for discovery at $\geq 2\sigma$; see Fig. 14 for results at $\geq 3\sigma$. Even in the presence of a medium-sized background, DM discovery might be possible. See Sec. IV B for details.

A. Overview

The distinct angular distribution of UHE neutrinos from DM decay—peaked towards the GC—provides a smoking-gun signature of their origin when compared to the isotropic flux of astrophysical and cosmogenic neutrinos. Yet, so far, the usefulness of this difference has gone underused or ignored in forecasts of searches for DM decay in UHE neutrino telescopes; see, e.g., Ref. [148]. In contrast, our methods embrace it. Unlike previous forecasts, we use this angular difference to not only claim the discovery of UHE neutrinos with a *possible* origin in DM decay, but to *assert* their DM origin in the presence of a non-DM neutrino background, i.e., to firmly discover UHE neutrinos from DM decay.

However, a sensible DM discovery claim requires a sufficiently large excess towards the GC. Added to that, if there is a large isotropic background of non-DM neutrinos, it could wash out the excess of neutrinos from DM decay, weakening the discovery claim.
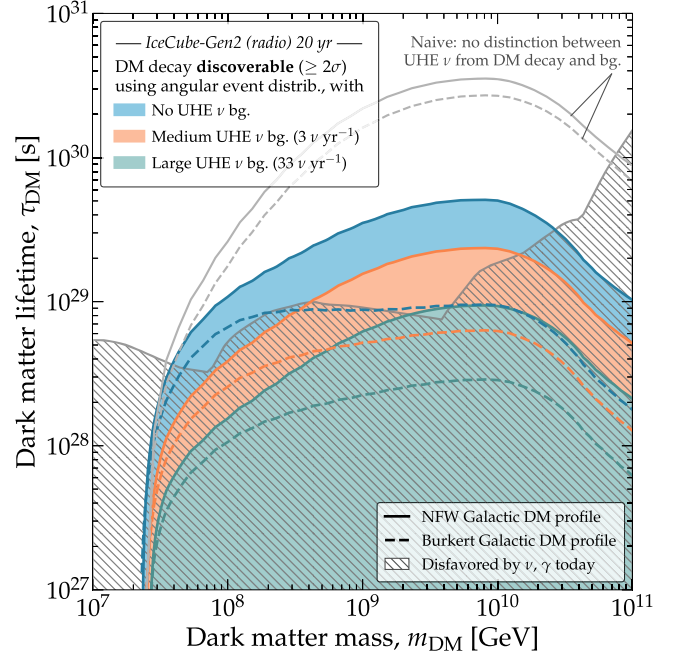
FIG. 8. Discovery prospects of UHE neutrinos from DM decay for NFW vs Burkert Galactic DM profiles. Same as Fig. 7, but comparing results obtained using the NFW vs Burkert Galactic DM density profiles (Fig. 3). Results are for discovery at $\geq 2\sigma$ after 20 years; see Fig. 16 for more results using the Burkert profile. Existing lower limits on the DM lifetime are the same as in Fig. 1, and computed assuming the NFW profile [48]. If the Galactic DM profile is puffy, like the Burkert profile, then discovery of DM becomes barely feasible, and only if there is no isotropic non-DM UHE neutrino background. See Sec. IV B for details.

In our forecasts below, we quantify the above statements in two ways. First (Sec. IV B), we find the values of the mass and lifetime of DM needed to discover UHE neutrinos from its decay, in the presence of a non-DM neutrino background. For this, we use only the angular distribution of detected events in the radio array of IceCube-Gen2. Second (Sec. IV C), in the event of discovery, we illustrate the accuracy with which the DM mass and lifetime could be measured. For this, we use the joint angular and energy distribution of events.

B. Discovery prospects

We forecast the regions of DM mass and lifetime where UHE neutrinos from DM decay could be discovered. Figure 7 (also Fig. 14) shows our results.

1. Statistical methods

We produce discovery forecasts by analyzing projected samples of detected events. To be conservative, we use only their angular distribution, summed over all energies, since it is in it that the critical difference between the flux of neutrinos from DM decay and the non-DM neutrino
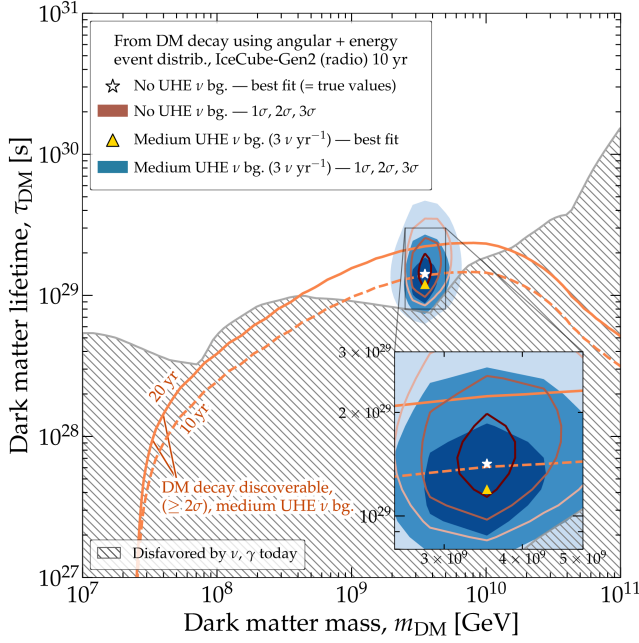
FIG. 9. DM mass and lifetime inferred from detecting UHE neutrinos from DM decay in the radio array of IceCube-Gen2. Results are generated for an illustrative choice of the true values of the DM mass and lifetime, $m_{\mathrm{DM}} = 3.5 \times 10^9$ GeV and $\tau_{\mathrm{DM}} = 1.19 \times 10^{29}$ s, which are representative of what is discoverable with 10 years of detector exposure and allowed by present-day limits (Fig. 7). Forecasts are for two choices of the background isotropic flux of non-DM UHE neutrinos: null and medium (Sec. II A), i.e., 10% of the cosmogenic flux by Bergman & van Vliet [103] (Fig. 2). The forecasts use the joint angular and energy distribution of events, and baseline choices of the detector angular and (logarithmic) energy resolution, $\sigma_\Omega = 3°$ and $\sigma_\epsilon = 0.1$; see Sec. III B. This figure assumes the NFW density profile for Galactic DM. Existing lower limits on the DM lifetime are the same as in Fig. 1. In the event of DM discovery, the DM mass and lifetime may be measured with reasonable accuracy and precision. See Sec. IV C for details.
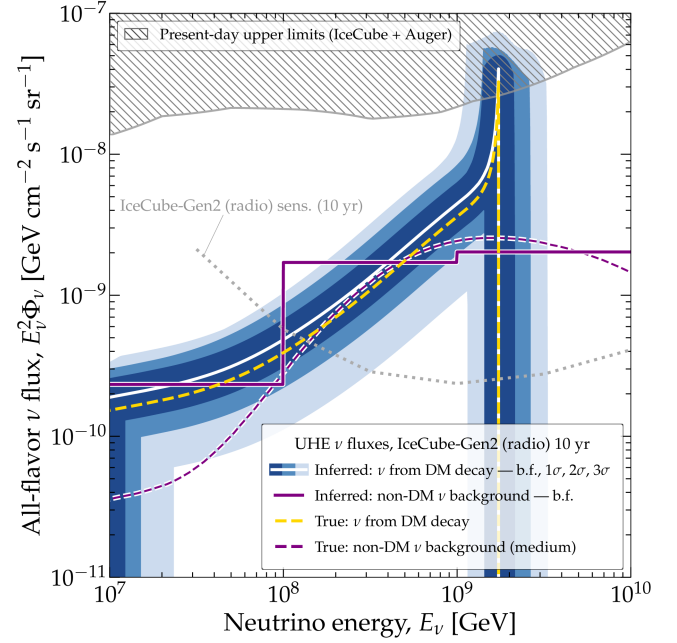
FIG. 10. Inferred flux of UHE neutrinos using the radio array of IceCube-Gen2. The flux of neutrinos from DM decay, sky-averaged, and the isotropic background flux are shown separately. The true values of the DM mass and lifetime are the same as used in Fig. 9. The allowed band of neutrino flux from DM decay corresponds to the allowed regions of inferred DM mass and lifetime from Fig. 9. The forecast assumes our medium-sized benchmark background flux of non-DM UHE neutrinos (Sec. II A), i.e., 10% of the cosmogenic neutrino flux by Bergman & van Vliet [103] (Fig. 2), or about three background events detected per year. This figure assumes the NFW density profile for Galactic DM. Existing upper limits on the flux of UHE neutrinos are from IceCube [91] and Auger [147]. The projected sensitivity of the radio array of IceCube-Gen2 is from Ref. [149]. Even using a coarse model for the UHE neutrino flux background [Eq. (18)], the flux of neutrinos from DM decay may be reconstructed with reasonable accuracy and precision. See Sec. IV C for details.

background manifests (Sec. II C). Later (Sec. V), we derive upper limits using also their energy distribution. We build our forecasts using the maximum likelihood technique and report mean discovery prospects based on Asimov data samples.

Each event sample is the sum of events due to neutrinos from DM decay, dependent on the DM mass, m_{DM}, and lifetime, τ_{DM}, and events from the background of non-DM neutrinos, rescaled by a flux normalization, $\mathcal{N}_\Phi$, i.e.,

$$\frac{dN_\nu(\boldsymbol{\vartheta})}{d\Omega^{\mathrm{rec}}} = \frac{dN_\nu^{\mathrm{DM}}(m_{\mathrm{DM}}, \tau_{\mathrm{DM}})}{d\Omega^{\mathrm{rec}}} + \mathcal{N}_\Phi \frac{dN_\nu^{\mathrm{bg}}}{d\Omega^{\mathrm{rec}}}, \quad (11)$$

where $\boldsymbol{\vartheta} \equiv \{m_{\mathrm{DM}}, \tau_{\mathrm{DM}}, \mathcal{N}_\Phi\}$. For the non-DM background, we show forecasts obtained under the three benchmark scenarios presented in Sec. II A: a large flux set to the cosmogenic flux by Bergman & van Vliet [103], a medium

flux that is 10% of that, and a null background; see Fig. 2. The large and medium benchmark backgrounds have the same angular distribution of events (see Fig. 6 and also Fig. 4 in Ref. [74]); they only differ in the total number of events (Fig. 5).

Based on a projected event sample, we compare two hypotheses: the DM hypothesis, where the angular distribution of events is best explained by the presence of a DM decay component on top of a background non-DM component vs the null hypothesis, where it is best explained by the presence of only the background non-DM component. In both cases, the background flux normalization, $\mathcal{N}_\Phi$, is left free to vary to best fit the data. Hence, when analyzing a simulated event sample, we obtain results that do not require prior knowledge of the true background flux. We do this separately for each of the three above choices of the

simulated background flux, and for a wide range of true values of the DM and lifetime.

First, for a particular choice of the true DM mass and lifetime, m_{DM} and τ_{DM}, and using the true value of the flux normalization, $\mathcal{N}_\Phi = 1$, we compute the projected *observed* sample of N_{evts} events, each with reconstructed direction Ω_i^{rec} sampled from the distribution $dN_\nu(m_{DM}, \tau_{DM}, \mathcal{N}_\Phi = 1)/d\Omega^{rec}$. Later, we use a test statistic that is averaged over all possible random realizations of the number of events and of the distribution of reconstructed directions of the events.

Then, based on this observed sample, we evaluate an unbinned likelihood function at different test values of the model parameters, $\boldsymbol{\vartheta}' \equiv (m'_{DM}, \tau'_{DM}, \mathcal{N}'_\Phi)$, i.e.,

$$\mathcal{L}(\boldsymbol{\vartheta}'; \{\Omega_i^{rec}\}) = e^{-N_\nu(\boldsymbol{\vartheta}')} \prod_{i=1}^{N_{evts}} \frac{dN_\nu(\boldsymbol{\vartheta}')}{d\Omega^{rec}}\bigg|_{\Omega_i^{rec}}, \quad (12)$$

where $N_\nu(\boldsymbol{\vartheta}') \equiv \int (dN_\nu(\boldsymbol{\vartheta}')/d\Omega^{rec}) d\Omega^{rec}$ is the all-sky event rate. In the comparison, we let the test values of m'_{DM}, τ'_{DM}, and $\mathcal{N}'_\Phi$ float as free parameters, as they would in a test based on real experimental data. Under the null hypothesis, where there is no DM decay contribution because DM is stable (i.e., $\tau_{DM} \to \infty$), the likelihood reduces to

$$\mathcal{L}_{bg}(\mathcal{N}'_\Phi; \{\Omega_i^{rec}\}) \equiv \lim_{\tau'_{DM} \to \infty} \mathcal{L}(\boldsymbol{\vartheta}'; \{\Omega_i^{rec}\}), \quad (13)$$

where the right-hand side no longer depends on the test values m'_{DM} and τ'_{DM}.

For a specific choice of the true values of m_{DM} and τ_{DM}, the test statistic depends on the angular distribution of the associated random observed event sample. To account for the possible different realizations of the observed sample, we average the logarithm of the likelihood functions, Eqs. (12) and (13), over all possible realizations. The probability to observe a total number of N_{evts}, over the full sky, $\mathcal{P}(N_{evts}|N_\nu)$, is given by a Poisson distribution with a mean value equal to the mean all-sky event rate, $N_\nu \equiv N_\nu(m_{DM}, \tau_{DM}, \mathcal{N}_\Phi = 1)$. The probability to sample an event with reconstructed direction Ω_i^{rec} from this distribution is $\mathcal{P}(\Omega_i^{rec}) \equiv (1/N_\nu)(dN_\nu/d\Omega^{rec})|_{\Omega_i^{rec}}$. Thus, the likelihood function, Eq. (12), averaged over all possible realizations of the event sample, is

$$\langle \ln \mathcal{L}(\boldsymbol{\vartheta}') \rangle_{m_{DM}, \tau_{DM}}$$

$$= \sum_{N_{evts}=0}^{\infty} \mathcal{P}[N_{evts}|N_\nu(m_{DM}, \tau_{DM}, \mathcal{N}_\Phi = 1)]$$

$$\times \int d\Omega_1^{rec} \cdots \int d\Omega_{N_{evts}}^{rec} \prod_{i=1}^{N_{evts}} \mathcal{P}(\Omega_i^{rec}|m_{DM}, \tau_{DM}, \mathcal{N}_\Phi = 1)$$

$$\times \ln \mathcal{L}[\boldsymbol{\vartheta}', \{\Omega_j^{rec}\}_{j=1}^{N_{evts}}], \quad (14)$$

and, similarly, the average log-likelihood under the null hypothesis, in which only background non-DM neutrinos are present, Eq. (13), is

$$\langle \ln \mathcal{L}_{bg}(\mathcal{N}'_\Phi) \rangle_{m_{DM}, \tau_{DM}} \equiv \lim_{\tau'_{DM} \to \infty} \langle \ln \mathcal{L}(\boldsymbol{\vartheta}') \rangle_{m_{DM}, \tau_{DM}}. \quad (15)$$

We average the log-likelihood, rather than the likelihood, to prevent the averaging procedure from prescribing exceedingly large averaging weights to random realizations that have associated large likelihood values. This corresponds to obtaining the results for an Asimov data sample [181], in which the observed distribution of events exactly coincide with the expected one.

To compare the two hypotheses, we use as a test statistic the average log-likelihood ratio, i.e.,

$$\langle \Lambda(m_{DM}, \tau_{DM}) \rangle = \min_{\mathcal{N}'_\Phi} [-2\langle \ln \mathcal{L}_{bg}(\mathcal{N}'_\Phi) \rangle_{m_{DM}, \tau_{DM}}]$$
$$- \min_{\boldsymbol{\vartheta}'} [-2\langle \ln \mathcal{L}(\boldsymbol{\vartheta}') \rangle_{m_{DM}, \tau_{DM}}]. \quad (16)$$

According to Wilks' theorem [182], in the asymptotic limit of a large data sample, this quantity follows an χ^2 distribution with 2 degrees of freedom, corresponding to the difference between the dimensions of the parameter spaces of the two competing hypotheses. We adopt it in our forecasts since, for 10 and 20 years of detector exposure and for the neutrino fluxes that we adopt, they are based on a large number of events. Hence, below, when $\langle \Lambda \rangle > 6$, we claim discovery of DM neutrinos at the 2σ confidence level (CL); when $\langle \Lambda \rangle > 11.5$, we claim it at 3σ C.L.

2. Results

Figure 7 shows the regions of DM mass and lifetime, obtained with the above methods, where DM can be discovered at $\geq 2\sigma$. We show results for our three benchmark choices of non-DM UHE neutrino background flux (Sec. II A)—null, medium, and large. The results in Fig. 7 convey three key messages.

First, while a large part of the parameter space in Fig. 7 is already disfavored by present-day neutrino and gamma-ray searches, upcoming UHE neutrino telescopes will extend the search to longer DM lifetimes, roughly above 10^{29} s, that are unreachable with present-day experiments. This aspect of our results agrees with previous works; see, e.g., Refs. [48,148]). Yet, for the first time, we fortify the claim by showing that it holds even in the presence of a medium-sized isotropic background flux of non-DM UHE neutrinos.

Second, Fig. 7 shows the significant difference between *detecting* events, which *a priori* may or may not be due to DM decay, and *claiming* that those events are produced by DM decay. Earlier forecasts of UHE neutrino detection from DM decay [148] had only investigated the maximum lifetime needed to detect neutrinos from DM decay, without identifying their origin. We show a version of these

forecasts in Fig. 7, generated by demanding that DM decay yields at least one event over the full sky, background-free, with a probability larger than 95% (or 99.7% in Fig. 14). As expected, this weaker criterion leads to overly long lifetimes being discoverable: compared to our results using the angular distribution of events, lifetimes longer by at least 1 order of magnitude could be detected without actually leading to a DM discovery. Thus, hereafter the main observations and conclusions of our work are based exclusively on forecasts made using the angular—and energy (in Secs. IV C and V)—distribution of events.

Third, Fig. 7 shows that, while the discovery prospects are best when background-free, as expected, the presence of a medium-size background only degrades the reach of discoverable DM lifetimes by a factor of about 2. In other words, UHE neutrinos retain the potential to reveal DM decay even in the presence of a sizable isotropic background of non-DM origin. This is true also for discovery at 3σ; see Fig. 14.

Figure 8 shows that, however, our prospects for discovery of DM decay are contingent on the Galactic DM density profile being cuspy, i.e., markedly pronounced towards the GC. Swapping the cuspy NFW profile for the puffy Burkert profile reduces the region amenable for discovery by about 1 order of magnitude, pushing it into the region of DM mass and lifetime that is already disfavored, and rendering discovery all but unfeasible. A subtle point is that the present-day disfavored region shown in Fig. 8 was computed, in Ref. [48], assuming the NFW profile. Assuming the Burkert instead would push down the disfavored region, leaving slightly more room for discovery under the Burkert profile; we do not attempt this recalculation here. Yet, the bottom line holds: for realistic choices of the detector angular resolution, like the $\sigma_\Omega = 3°$ that we adopt, the discovery of DM decay into UHE neutrinos will be likely only if the Galactic DM density profile is cuspy.

C. Measuring dark matter mass and lifetime

In the event of the discovery of DM decay into UHE neutrinos, we forecast how well the DM mass and lifetime could be inferred. Figure 9 shows our results.

1. Statistical methods

Above (Sec. IV B), we showed that to claim the discovery of DM decay into UHE neutrinos it was enough to use the angular distribution of events. In the event of discovery, inferring the DM lifetime also relies mainly on the angular distribution events, concretely, as before, on its excess towards the GC. Because the DM lifetime determines the normalization of the neutrino flux from DM decay, its value can be inferred from the magnitude of the excess. However, inferring the DM mass requires the energy distribution of events, too. Using it allows us to infer the DM mass by looking for the distinct bumplike feature imprinted by DM decay on the neutrino spectrum,

which peaks at $E_\nu = m_{\rm DM}/2$; see Figs. 2 and 5. Thus, below, we extend the statistical methods from Sec. IV B 1 to include also the energy of the detected events.

First, we generate the *true* event sample, i.e., the one that we assume will be detected. We use a procedure similar to the one we used to compute discovery prospects (Sec. IV B), but extended to included also the energy distribution of events. To illustrate our method, we choose $m_{\rm DM} = 3.5 \times 10^9$ GeV and $\tau_{\rm DM} = 1.19 \times 10^{29}$ s as true values; these are representative of the discoverable region under our benchmark medium non-DM in Fig. 7. We use for the non-DM background UHE neutrino flux the same three benchmarks (Sec. II A) that we used earlier to make discovery forecasts—null, medium, and large. In analogy to Eq. (11), the true distribution is

$$\frac{dN_\nu^{\rm true}(m_{\rm DM}, \tau_{\rm DM})}{dE_{\rm sh}^{\rm rec} d\Omega^{\rm rec}} = \frac{dN_\nu^{\rm DM}(m_{\rm DM}, \tau_{\rm DM})}{dE_{\rm sh}^{\rm rec} d\Omega^{\rm rec}} + \frac{dN_\nu^{\rm bg}}{dE_{\rm sh}^{\rm rec} d\Omega^{\rm rec}}.$$

(17)

From it, we randomly sample $N_{\rm evts}$ events, each with reconstructed energy $E_{{\rm sh},i}^{\rm rec}$ and direction $\Omega_i^{\rm rec}$. Later, for each choice of $m_{\rm DM}$ and $\tau_{\rm DM}$, we average our test statistic over all possible random realizations of the event samples.

Then we compare the true event sample to *test* event samples, generated for many different test values of DM mass and lifetime, in order to find which ones fit best. To produce test event samples, we generalize what we did to compute discovery prospects and adopt a generic model of the non-DM background neutrino energy spectrum. We parametrize it as a piecewise (pw) spectrum $\propto E_\nu^{-2}$, with three independent normalization constants, $\mathcal{N}_{\Phi,1}$, $\mathcal{N}_{\Phi,2}$, $\mathcal{N}_{\Phi,3}$, in three decades of neutrino energy, from 10^7 GeV to 10^{10} GeV. For ν_α, this is

$$\Phi_{\nu_\alpha}^{\rm bg-pw}(E_\nu) = \frac{f_{\alpha,\oplus}}{2E_\nu^2} \times \begin{cases} \mathcal{N}_{\Phi,1}, & 10^7 \leq E_\nu/{\rm GeV} < 10^8 \\ \mathcal{N}_{\Phi,2}, & 10^8 \leq E_\nu/{\rm GeV} < 10^9 \\ \mathcal{N}_{\Phi,3}, & 10^9 \leq E_\nu/{\rm GeV} \leq 10^{10} \end{cases},$$

(18)

where, for the flavor composition at Earth, we adopt the one from the canonical expectation of neutrino production via the pion decay chain (Sec. II A), computed using recent best-fit values of the neutrino mixing parameters [183,184], $f_{e,\oplus} = 0.298$, $f_{\mu,\oplus} = 0.359$, and $f_{\tau,\oplus} = 0.342$, from Ref. [185], i.e., close to flavor equipartition (see also, e.g., Ref. [186]). Since we make forecasts for 10–20 years, when the values of the mixing parameters will likely be known precisely [89], we neglect the small uncertainties in these predictions; see Eqs. (7)–(9) in Ref. [89]. The fluxes of ν_α and $\bar{\nu}_\alpha$ are identical; this is ensured by the factor of 2 in the denominator of Eq. (18).

We adopt this background flux model to analyze projected event samples using a phenomenological prescription of the non-DM neutrino background that is as agnostic as possible regarding the shape of its energy spectrum and its origin. Our strategy resembles one that would be used by future analyses based on real experimental observations. Indeed, similar flux models are used by the IceCube Collaboration to analyze present-day data [31,104]. Using the piecewise background flux, we compute the associated differential event spectrum, $dN_\nu^{\mathrm{bg-pw}}/dE_{\mathrm{sh}}^{\mathrm{rec}}d\Omega^{\mathrm{rec}}$, using the methods from Sec. III B. Thus, the total differential test event spectrum is

$$\frac{dN_\nu^{\mathrm{test}}(\boldsymbol{\vartheta}')}{dE_{\mathrm{sh}}^{\mathrm{rec}}d\Omega^{\mathrm{rec}}} = \frac{dN_\nu^{\mathrm{DM}}(m'_{\mathrm{DM}},\tau'_{\mathrm{DM}})}{dE_{\mathrm{sh}}^{\mathrm{rec}}d\Omega^{\mathrm{rec}}} + \frac{dN_\nu^{\mathrm{bg-pw}}(\mathcal{N}'_{\Phi,1},\mathcal{N}'_{\Phi,2},\mathcal{N}'_{\Phi,3})}{dE_{\mathrm{sh}}^{\mathrm{rec}}d\Omega^{\mathrm{rec}}}, \quad (19)$$

where now $\boldsymbol{\vartheta}' \equiv (m'_{\mathrm{DM}},\tau'_{\mathrm{DM}},\mathcal{N}'_{\Phi,1},\mathcal{N}'_{\Phi,2},\mathcal{N}'_{\Phi,3})$.

In analogy to Eq. (12), we evaluate an unbinned likelihood function at different test values of the model parameters, $\boldsymbol{\vartheta}'$, i.e.,

$$\mathcal{L}_{\mathrm{mea}}(\boldsymbol{\vartheta}',\{E_{\mathrm{sh},i}^{\mathrm{rec}},\Omega_i^{\mathrm{rec}}\}) = e^{-N_\nu^{\mathrm{test}}(\boldsymbol{\vartheta}')} \prod_{i=1}^{N_{\mathrm{evts}}} \frac{dN_\nu^{\mathrm{test}}(\boldsymbol{\vartheta}')}{dE_{\mathrm{sh}}^{\mathrm{rec}}d\Omega^{\mathrm{rec}}}\bigg|_{E_{\mathrm{sh},i}^{\mathrm{rec}},\Omega_i^{\mathrm{rec}}}, \quad (20)$$

where N_ν^{test} is the all-sky number of events with energies $E_{\mathrm{sh}}^{\mathrm{rec}} \geq 10^7$ GeV. As before (Sec. IV B), for a specific choice of the true values of m_{DM} and τ_{DM} and of the non-DM background neutrino flux, we average the logarithm of the above likelihood over all possibly random realizations of the observed event sample. In analogy to Eq. (14), this yields $\langle \ln \mathcal{L}_{\mathrm{mea}}(\boldsymbol{\vartheta}') \rangle_{m_{\mathrm{DM}},\tau_{\mathrm{DM}}}$. Finally, to infer the values of the DM mass and lifetime, we profile the likelihood over the test parameters and, in analogy to Eq. (16), define the test statistic

$$\begin{aligned}
&\langle \Lambda_{\mathrm{mea}}(m_{\mathrm{DM}},\tau_{\mathrm{DM}}) \rangle \\
&= \min_{\mathcal{N}'_{\Phi,1},\mathcal{N}'_{\Phi,2},\mathcal{N}'_{\Phi,3}}[-2\langle \ln \mathcal{L}_{\mathrm{mea}}(m'_{\mathrm{DM}}=m_{\mathrm{DM}}, \\
&\quad \tau'_{\mathrm{DM}}=\tau_{\mathrm{DM}},\mathcal{N}'_{\Phi,1},\mathcal{N}'_{\Phi,2},\mathcal{N}'_{\Phi,3})\rangle_{m_{\mathrm{DM}},\tau_{\mathrm{DM}}}] \\
&\quad - \min_{\boldsymbol{\vartheta}'}[-2\langle \ln \mathcal{L}_{\mathrm{mea}}(\boldsymbol{\vartheta}') \rangle_{m_{\mathrm{DM}},\tau_{\mathrm{DM}}}]. \quad (21)
\end{aligned}$$

As in Sec. IV B, based on Wilks' theorem, this test statistic follows an χ^2 distribution with 2 degrees of freedom. Below, we use it to infer allowed regions of m_{DM} and τ_{DM} at different confidence levels.

2. Results

Figure 9 illustrates that, in the event of discovery of DM decay into UHE neutrinos, IceCube-Gen2 may infer the values of the DM mass and lifetime responsible for the discovered signal. In Fig. 9, we show results obtained using our illustrative choice for the true DM and mass lifetime (see above). To illustrate the influence of a non-DM isotropic background flux of UHE neutrinos, we compare results obtained assuming no background vs assuming our medium benchmark background (Sec. II A).

Our results confirm our expectation (Sec. IV C 1) that using the energy distribution of events grants us sensitivity to the DM parameters. For the choice of DM mass and lifetime in Fig. 9, and similar ones, their values can be inferred with an accuracy of a factor of 2–3. In the presence of the medium background, the accuracy degrades only slightly compared to the null-background case. A larger background degrades the accuracy further, but does not preclude measurement; it may, however, reduce the precision with which the DM mass is inferred (see below).

While the accuracy on the DM mass is only weakly degraded by the presence of a background, the precision on it suffers more appreciably. In the absence of a background, the best-fit value of the DM mass matches its true value. In the presence of a medium-size background, its best-fit value is offset from the real one. This stems from our choice of the three-piece background flux, Eq. (18), to analyze projected event samples. On the one hand, this flux prescription frees us from having to rely on specific theoretical predictions of the UHE astrophysical or cosmogenic neutrino flux. On the other hand, because it is rather coarse—with decade-wide flux normalization constants—it fails to reproduce closely the shape of the background neutrino energy spectrum, Fig. 2. Even so, the mismatch between the best-fit and true values is small; they are consistent within 1σ. Future analyses could mitigate this loss of precision by adopting a more finely binned version of the piecewise background flux.

Thus, the DM mass and lifetime can be accurately inferred, even in the presence of a non-DM isotropic background flux of UHE neutrinos, by analyzing jointly the angular and energy distribution of events. In doing so, there is essentially no degeneracy between the flux of UHE neutrinos from DM decay and the unknown background flux of UHE astrophysical and cosmogenic neutrinos, since in our procedure the former is determined almost exclusively by neutrinos from the GC, while the latter is determined by neutrinos from every direction.

Figure 10 shows the corresponding allowed regions of the sky-averaged diffuse flux of UHE neutrinos from DM. The approximate factor-of-2 uncertainty on the DM lifetime translates into an uncertainty of similar size on the flux normalization. The mismatch between the best-fit and true vales of the DM mass translates into a mismatch between the low-energy tails of secondary neutrinos from electroweak corrections in their corresponding fluxes. Figure 10 shows also that our piecewise background flux model, Eq. (18), is able to match the true background flux

reasonably well, within the limitations of its coarse shape, except in the lowest energy bin, where the match is poor due to the background flux dipping well below the sensitivity of the radio array of IceCube-Gen2, thus leading to low event rates. There, results could be improved by a combined analyses of TeV–PeV and UHE neutrinos detected, respectively, by the optical and radio arrays of IceCube-Gen2 [63,187].

V. PROJECTED BOUNDS ON DARK MATTER DECAY

The lifetime of heavy DM that decays into UHE neutrinos may be bound even in the presence of sizable non-DM neutrino backgrounds, by using the joint angular and energy distribution of detected events, in 10 years of exposure of the radio array of IceCube-Gen2 (Fig. 11). Even when using the largest possible allowed background, the bounds on the DM lifetime remain competitive or better than present-day bounds (Fig. 12).

A. Overview

Absent evidence for UHE neutrinos from DM decay, it may still be possible to place competitive bounds on the DM lifetime, even in the presence of a sizable non-DM isotropic UHE neutrino background flux. Like for the discovery of DM decay (Sec. IV), below we gear our results for radio detection at IceCube-Gen2, but our methods and, broadly stated, our conclusions are applicable to next-generation UHE neutrino telescopes, in general.

References [48,71,148] reported projected bounds for DM decay into UHE neutrinos, including via their radio detection at IceCube-Gen2. We improve on those in two ways. First, we use a significantly more detailed calculation of event rates in IceCube-Gen2, based on state-of-the-art simulations of neutrino propagation, interaction, and radio detection (Sec. III). Like for the discovery of DM decay, this is key to generating reliable angular and energy event distributions, which our analysis uses to discriminate against the background. Second, unlike previous works, we forecast bounds in the presence of a sizable non-DM isotropic UHE neutrino background flux. Reference [148] did consider the presence of a potential background, but discriminated against it simply by counting only neutrinos with energy smaller than $m_{\mathrm{DM}}/2$. In contrast, we use a full-fledged angular and energy analysis to produce our bounds.

B. Statistical methods

Unlike our earlier analyses to discover DM decay and infer the DM mass and lifetime (Sec. IV), to place bounds on DM decay we assume that the *true* observed event distributions are due solely to the non-DM isotropic background flux of UHE neutrinos, and we contrast *test* event distributions expected from DM decay against it. For the non-DM background flux, we use our two medium and

large benchmark fluxes (Sec. II A), based off of the cosmogenic neutrino flux by Bergman & van Vliet [103]. Our main conclusions hold for other choices of background, and we point out below what features of our results are due to our specific benchmark choices.

Further, unlike when computing discovery prospects (Sec. IV B), when setting bounds below we use not only the angular distribution of events, but also their energy distribution. We demand that the energy distribution of events lacks features that are characteristic of the energy spectrum of neutrinos from DM decay, i.e., a clustering of events with similar energies that reflects an underlying bumplike shape of the spectrum (Sec. II B). Admittedly, this is a broad conservative criterion: it discriminates against the flux of neutrinos from DM decay, but also against any astrophysical or cosmogenic flux that has a bumplike feature in its spectrum, of which there are many proposals, including our benchmark background fluxes; see, e.g., Fig. 2 in Ref. [74].

For a given choice of the non-DM neutrino background, we compute the true observed event distribution,

$$\frac{dN_\nu^{\mathrm{true}}}{dE_{\mathrm{sh}}^{\mathrm{rec}} d\Omega^{\mathrm{rec}}} = \frac{dN_\nu^{\mathrm{bg}}}{dE_{\mathrm{sh}}^{\mathrm{rec}} d\Omega^{\mathrm{rec}}}, \qquad (22)$$

using the methods from Sec. III C. From it, we sample random realizations of the observed event sample, consisting of a random number N_{evts} of events, each with reconstructed energy and direction, $E_{\mathrm{sh},i}^{\mathrm{rec}}$ and Ω_i^{rec}.

Then, for a choice of the DM mass m_{DM} and lifetime τ_{DM}, we compare the true event rate vs the test event rate expected from DM decay, $dN_\nu^{\mathrm{test}}(\boldsymbol{\vartheta}')/dE_{\mathrm{sh}}^{\mathrm{rec}} d\Omega^{\mathrm{rec}}$, given by Eq. (19) evaluated at test parameters $\boldsymbol{\vartheta}' \equiv (m'_{\mathrm{DM}} = m_{\mathrm{DM}}, \tau'_{\mathrm{DM}} = \tau_{\mathrm{DM}}, \mathcal{N}'_{\Phi,1}, \mathcal{N}'_{\Phi,2}, \mathcal{N}'_{\Phi,3})$. This test event rate is computed using the same piecewise background UHE neutrino spectrum, Eq. (18), that we used to infer the DM mass and lifetime (Sec. IV C).

Like when computing discovery forecasts, we compare the true (i.e., background-only) and test (i.e., background plus DM) hypotheses via an unbinned likelihood, given by Eq. (20), i.e.,

$$\mathcal{L}_{\mathrm{full}}(\boldsymbol{\vartheta}', \{E_{\mathrm{sh},i}^{\mathrm{rec}}, \Omega_i^{\mathrm{rec}}\}) = e^{-N_\nu^{\mathrm{test}}(\boldsymbol{\vartheta}')} \prod_{i=1}^{N_{\mathrm{evts}}} \frac{dN_\nu^{\mathrm{test}}(\boldsymbol{\vartheta}')}{dE_{\mathrm{sh}}^{\mathrm{rec}} d\Omega^{\mathrm{rec}}}\bigg|_{E_{\mathrm{sh},i}^{\mathrm{rec}}, \Omega_i^{\mathrm{rec}}}, \qquad (23)$$

which relies on the full available information on the events, i.e., their joint angular and energy distribution.

In addition, to highlight the role of the angular and energy information in placing bounds, we compute, separately, analyses that use limited information. An analysis that relies only on angular information uses a likelihood where the event rate is integrated across all reconstructed energies from 10^7 GeV to 10^{10} GeV, i.e.,

$$\mathcal{L}_{\rm ang}(\boldsymbol{\vartheta}', \{\Omega_i^{\rm rec}\}) = e^{-N_\nu^{\rm test}(\boldsymbol{\vartheta}')} \prod_{i=1}^{N_{\rm evts}} \left(\int dE_{\rm sh}^{\rm rec} \frac{dN_\nu^{\rm test}(\boldsymbol{\vartheta}')}{dE_{\rm sh}^{\rm rec} d\Omega^{\rm rec}} \right) \Bigg|_{\Omega_i^{\rm rec}}.$$

(24)

An analysis that relies only on energy information uses a likelihood where the event rate is all-sky, i.e.,

$$\mathcal{L}_{\rm en}(\boldsymbol{\vartheta}', \{E_{{\rm sh},i}^{\rm rec}\}) = e^{-N_\nu^{\rm test}(\boldsymbol{\vartheta}')} \prod_{i=1}^{N_{\rm evts}} \left(\int d\Omega^{\rm rec} \frac{dN_\nu^{\rm test}(\boldsymbol{\vartheta}')}{dE_{\rm sh}^{\rm rec} d\Omega^{\rm rec}} \right) \Bigg|_{E_{{\rm sh},i}^{\rm rec}}.$$

(25)

And, finally, an analysis that relies only on the all-sky number of events of all energies uses

$$\mathcal{L}_{\rm count}(\boldsymbol{\vartheta}') = e^{-N_\nu^{\rm test}(\boldsymbol{\vartheta}')} [N_\nu^{\rm test}(\boldsymbol{\vartheta}')]^{N_{\rm evts}}.$$

(26)

Like for the DM discovery prospects before, we compute projected bounds on the DM mass and lifetime using an Asimov event sample. In analogy to Eq. (14), we average the above likelihood functions over all possible random realizations of the observed events, sampled from the underlying event distribution due to the non-DM background, $dN_\nu^{\rm true}/dE_{\rm sh}^{\rm rec} d\Omega^{\rm rec}$. This yields the average functions $\langle \ln \mathcal{L}_{\rm full} \rangle$, $\langle \ln \mathcal{L}_{\rm ang} \rangle$, $\langle \ln \mathcal{L}_{\rm en} \rangle$, and $\langle \ln \mathcal{L}_{\rm count} \rangle$. In analogy to Eq. (15), we define likelihood functions computed under the background-only hypothesis, e.g.,

$$\langle \ln \mathcal{L}_{\rm full,bg}(\mathcal{N}_{\Phi,1}', \mathcal{N}_{\Phi,2}', \mathcal{N}_{\Phi,3}') \rangle$$
$$= \lim_{\tau_{\rm DM}' \to \infty} \langle \ln \mathcal{L}_{\rm full}(m_{\rm DM}', \tau_{\rm DM}', \mathcal{N}_{\Phi,1}', \mathcal{N}_{\Phi,2}', \mathcal{N}_{\Phi,3}') \rangle, \quad (27)$$

where the right-hand side no longer depends on the DM mass and lifetime. Similar expressions apply for the other likelihood functions, i.e., $\langle \mathcal{L}_{\rm ang,bg} \rangle$, $\langle \mathcal{L}_{\rm en,bg} \rangle$, $\langle \mathcal{L}_{\rm count,bg} \rangle$.

To place bounds, we follow Ref. [181] and define a test statistic that compares the true hypothesis—that there is no DM neutrino flux—and test hypothesis—that there is a DM neutrino flux with parameters $m_{\rm DM}$ and $\tau_{\rm DM}$. For example, for the full analysis,

$$\langle \Lambda_{\rm full}(m_{\rm DM}, \tau_{\rm DM}) \rangle = -2 \min_{\mathcal{N}_{\Phi,1}', \mathcal{N}_{\Phi,2}', \mathcal{N}_{\Phi,3}'}$$
$$\times [\langle \ln \mathcal{L}_{\rm full}(m_{\rm DM}, \tau_{\rm DM}, \mathcal{N}_{\Phi,1}', \mathcal{N}_{\Phi,2}', \mathcal{N}_{\Phi,3}') \rangle$$
$$- \langle \ln \mathcal{L}_{\rm full,bg}(\mathcal{N}_{\Phi,1}', \mathcal{N}_{\Phi,2}', \mathcal{N}_{\Phi,3}') \rangle] \Theta[\hat{\tau}_{\rm DM} - \tau_{\rm DM}], \quad (28)$$

where Θ is the Heaviside function and $\hat{\tau}_{\rm DM}(m_{\rm DM})$ is the value of the DM lifetime that, for a fixed value of the DM mass, $m_{\rm DM}$, maximizes the likelihood function $\langle \ln \mathcal{L}_{\rm full} \rangle$. Similar expressions apply for the other analyses, i.e., $\langle \Lambda_{\rm ang} \rangle$, $\langle \Lambda_{\rm en} \rangle$, $\langle \Lambda_{\rm count} \rangle$. With this definition, under the null hypothesis where neutrinos from DM decay exist, the test statistic should be distributed according to a half-χ^2 distribution with 1 degree of freedom. Hence, below, we

place limits on the DM lifetime at the 2σ C.L. when $\langle \Lambda_{\rm full} \rangle > 2.7$, and similarly for the other analyses.

C. Results

Figure 11 shows the resulting projected bounds on the DM lifetime, obtained by adopting our benchmark medium non-DM UHE neutrino background. We extract two main observations from it.

First, Fig. 11 shows that the existence of a sizable non-DM neutrino background appreciably weakens the bounds, compared to those obtained by plainly demanding that no
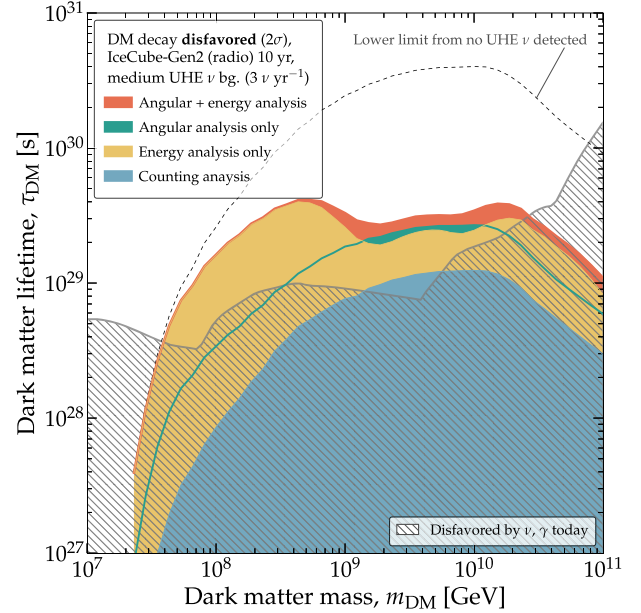

FIG. 11. Projected lower limits on the DM mass and lifetime from a search for UHE neutrinos in the radio array of IceCube-Gen2. The limits are placed in the absence of detection of neutrinos from DM decay, assuming a medium-sized benchmark non-DM isotropic background flux of UHE neutrinos, i.e., 10% of the cosmogenic neutrino flux by Bergman & van Vliet [103]; see Fig. 2. We show bounds obtained using the joint angular and energy distribution of events—our main results—only the angular or only the energy distribution, and only counting the all-sky rate of events of all energies. The bounds obtained using energy information dip between 10^9 and 10^{10} GeV, where our benchmark background neutrino energy spectrum peaks and may mimic the spectrum of neutrinos from DM decay. We adopt baseline choices of the detector angular and (logarithmic) energy resolution, $\sigma_\Omega = 3°$ and $\sigma_\epsilon = 0.1$; see Sec. III B. For comparison, we show limits obtained if no UHE neutrinos are detected at 2σ. This figure assumes the NFW density profile for Galactic DM. Existing lower limits on the DM lifetime are the same as in Fig. 1. Even in the presence of a sizable non-DM isotropic background flux of UHE neutrinos, using the angular and energy distributions of events keeps the projected lower limits on DM lifetime comparable to, or better than, present-day ones. See Fig. 15 for results obtained using a large UHE neutrino background. See Sec. V for details.

UHE neutrino is detected, which are representative of most previous analyses in the literature. (In Fig. 11, the null-detection curve also corresponds to a value of the test statistic of 2.7, which implies a mean number of detected events of 1.35.) Blatantly, when using only a counting analysis, the bounds that we obtain are up to 40 times weaker than bounds obtained from demanding that no neutrino is detected. In reality, how much the bounds are weakened will depend on the actual size and shape of the non-DM background. Still, our results serve as a reminder that projected bounds on the DM lifetime reported in the literature may be optimistic.

Second, Fig. 11 shows that using the angular and energy event distributions mitigate how much the bounds are weakened. Depending on the DM mass, they improve the bounds compared to the counting analysis by a factor of 2–10. This holds even when adopting our benchmark large background instead; see Fig. 15. Overall, using the angular and energy distributions allows projected bounds to remain competitive with present-day ones.

The angular and energy information complement each other. Using the energy distribution strongly improves the bounds at low and high DM masses. In the intermediate region, between 10^9 GeV and 10^{10} GeV, bounds that use energy information weaken because this is where our benchmark background neutrino spectrum peaks (Fig. 2) and where it may be misconstrued as being due to DM decay; see the discussion in Sec. V B. This is counteracted by using angular information: in the 10^9–10^{10} GeV range, where the detector response is largest (see Fig. 13 in Ref. [89]), the isotropic neutrino background induces a number of events large enough for the analysis to reject an excess towards the GC from DM decay. Figure 11 shows the result of this interplay for our particular choice of non-DM background; in reality, the specifics will depend on the actual size and shape of the background.

Figure 12 shows that using our large benchmark non-DM UHE neutrino background instead—10 times larger than the medium one—weakens the bounds by only a factor of roughly 2, except in the range 10^9–10^{10} GeV, where the bounds weaken by a factor of up to 6, but even so remain roughly competitive with present-day ones. This represents promising prospects: the background flux we use here [103] is as large as allowed by the present-day IceCube [91] and Auger [147] upper limits. Yet, even with this aggressive choice of background, our projected bounds in Fig. 12 remain comparable or better than present-day ones.

Figure 13 shows that, naturally, the bounds degrade when using the Burkert Galactic DM profile instead of the NFW profile. Because the Burkert profile is puffier, the bounds derived from the analysis of the angular distribution of events are weakened, so most of the limit-setting power comes from the energy distribution of events instead; see also Fig. 17. Still, the energy analysis sets bounds using the Burkert profile that are only a factor-of-2 worse than using the NFW profile. Thus, given our extant imperfect
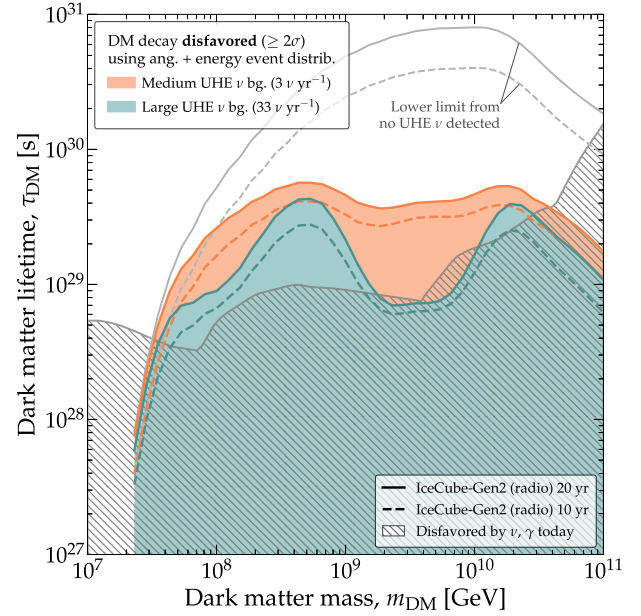

FIG. 12. Projected lower limits on the DM lifetime for different choices of non-DM UHE neutrino background. Same as Fig. 11, but showing only results obtained from the joint angular and energy analysis. We compare results obtained using our medium and large benchmark background isotropic fluxes of non-DM neutrinos (Fig. 2), and using 10 years and 20 years of detector exposure. The limit on DM lifetime is degraded for values of the DM mass that yield neutrino spectra that peak at energies where our benchmark background neutrino spectrum also peaks, i.e., between 10^9 and 10^{10} GeV. This figure assumes the NFW density profile for Galactic DM. The presence of a sizable non-DM isotropic background flux of UHE neutrinos will degrade the lower limits that can be placed on the DM lifetime, but only within a window of values of the DM mass. See Sec. V for details.

knowledge of the Galactic DM profile—in particular, given the possibility of a puffy DM profile—leveraging the interplay between energy and angular information is key.

VI. SUMMARY AND OUTLOOK

In the next decade, UHE neutrino telescopes, presently in planning, will deliver a new way to look for heavy DM, with masses in excess of 10^7 GeV, via its decay into UHE neutrinos, with energies in excess of 10^7 GeV. To properly harness this potential, it is critical to disentangle the signatures of UHE neutrinos of DM decay origin from the signatures of UHE neutrinos of astrophysical and cosmogenic origin—long sought but still undiscovered—that act as a background to DM searches. Failure to do so may incur in steep misrepresentation when claiming discovery of DM decay, inferring the DM mass and lifetime in the event of discovery, or setting bounds on the DM mass and lifetime, otherwise. The task is complicated by the fact that the size and shape of the non-DM neutrino background is unknown, that the number of detected events may be
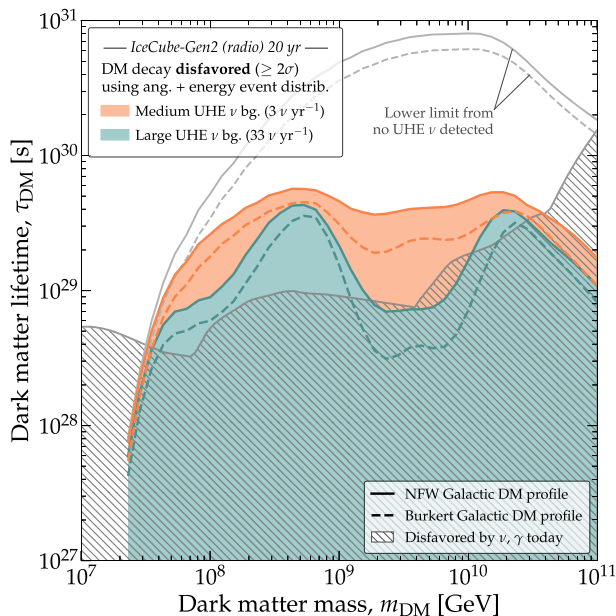
FIG. 13.   Projected lower limits on the DM lifetime for NFW vs Burkert Galactic DM profiles. Same as Fig. 12, but comparing results obtained using the NFW vs Burkert Galactic DM density profiles (see Fig. 3). In this figure, results are for discovery at $\geq 2\sigma$ after 20 years; see Fig. 17 for more results using the Burkert profile. If the Galactic DM profile is puffy, like the Burkert profile, then bounds weaken by a factor of roughly 2, compared to a cuspy DM profile, like NFW. See Sec. V for details.

small, and that the direction- and energy-measurement capabilities of the detectors are limited.

Even so, we have shown, by means of detailed forecasts, that these obstacles are surmountable. Key to that is to examine the energy and angular distributions of the detected UHE neutrinos. They grant us access to the essential differences between the diffuse neutrino fluxes from DM decay and from the non-DM background: in energy, the former is concentrated around the DM mass, while the latter is more spread out (Fig. 2), and, in direction, the former is concentrated around the GC—where DM is abundant—while the latter is isotropic (Fig. 4). In our forecasts, we look for these differences in projected observations.

We have geared our forecasts to the radio detection of UHE neutrinos in the envisioned IceCube-Gen2 neutrino telescope, which we simulate using state-of-the-art methods, including experimental nuances that dull the above differences between the fluxes. Our findings are promising: these differences survive an analysis under realistic experimental conditions (Figs. 5 and 6). Therefore, while the existence of a non-DM UHE neutrino background, even the largest presently allowed, weakens claims of discovery of DM decay or bounds on it, it does not necessarily preclude them. Still, the limit-setting potential and, particularly, the discovery potential are contingent to the Galactic DM profile peaking markedly towards the GC (Figs. 8 and 13).

Regarding the discovery of DM decay, we have shown that DM with mass between 10^8 GeV and 10^{10} GeV and lifetime of roughly 10^{29} s should be discoverable after 10 years of operation of the radio array of IceCube-Gen2, even in the presence of a medium-sized non-DM neutrino background that yields about three events per year (Fig. 7). This is conservatively achieved using only the angular distribution of detected events. Under a larger background, of about 33 events per year, discovery becomes unfeasible in the face of existing bounds on the DM lifetime. Our discovery forecasts depend only mildly on the shape of the energy spectrum of the non-DM neutrino background— whose size we let float in our analyses—and depend mainly on the total number of events.

In the event of discovery, the DM mass and lifetime could be measured with reasonable accuracy and precision (Fig. 9), depending on their true values, and the flux of UHE neutrinos from DM decay could be similarly inferred (Fig. 10). Importantly, this result is robust: when inferring the values of the DM parameters—and also when setting bounds on them (see below)—we analyze the simulated event samples *without* assuming knowledge of the shape and size of the energy spectrum of the non-DM neutrino background.

If discovery is not possible, we will be able to place lower limits on the DM lifetime, which we forecast. Using the joint angular and energy distribution of events allows us to constrain the presence of bumplike energy spectra and excesses towards the Galactic Center even under challenging, but plausible, scenarios where the energy spectrum of the non-DM neutrino background is medium-sized and whose bumplike energy spectrum inconveniently resembles that of neutrinos from DM decay (Fig. 11). Even in the presence of a large bumplike non-DM background, using the energy distribution of events safeguards the limits on the DM lifetime for DM masses sufficiently far from the peak of the non-DM flux (Fig. 12). Overall, we forecast lower limits on the DM lifetime that are comparable to, or better than, existing limits from gamma rays and TeV–PeV neutrinos.

While our forecasts are geared to the detection of UHE neutrinos in the radio array of IceCube-Gen2, our conclusions apply generally to planned neutrino telescopes of comparable size, radio-based, and otherwise, and our methods can be readily adapted to them. In particular, detectors with an envisioned high angular resolution, like GRAND, could be better at discovering or discriminating against an excess of events towards the GC [71].

It seems that, fortunately, the potential of next-generation UHE neutrino telescopes to probe heavy DM decay may be safeguarded against sizable unknown neutrino backgrounds.
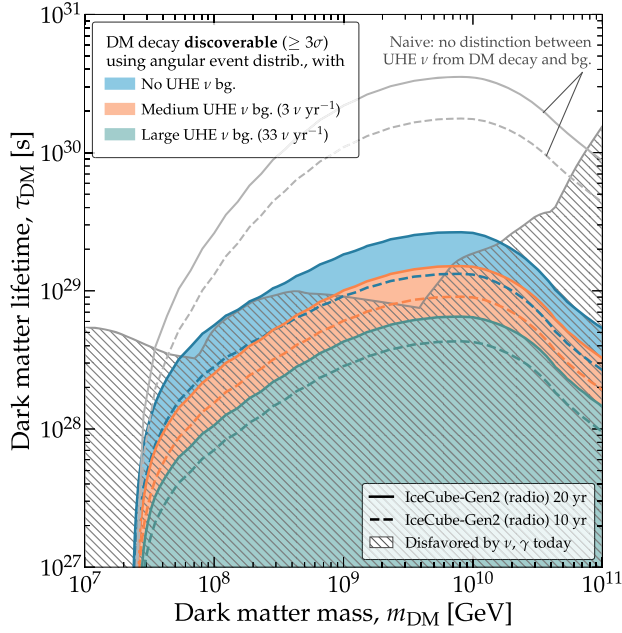
ACKNOWLEDGMENTS

FIG. 14. Discovery prospects for UHE neutrinos from DM decay, at $\geq 3\sigma$. Compare to Fig. 7, which is for $\geq 2\sigma$.
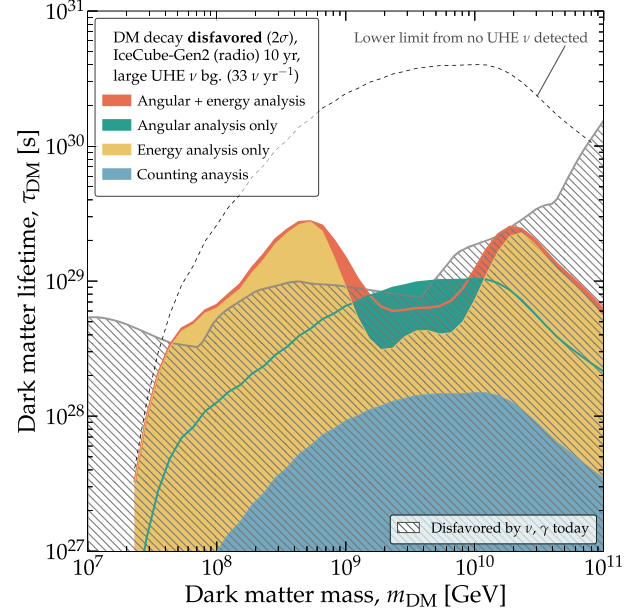
FIG. 15. Projected lower limits on the DM lifetime, under a large background of non-DM UHE neutrinos. Same as Fig. 15, but assuming our large benchmark non-DM isotropic background flux of UHE neutrinos, i.e., the cosmogenic neutrino flux by Bergman & van Vliet [103]. See Sec. V for details.

APPENDIX: ADDITIONAL FIGURES

Without further ado, we include additional figures to complement those in the main text:
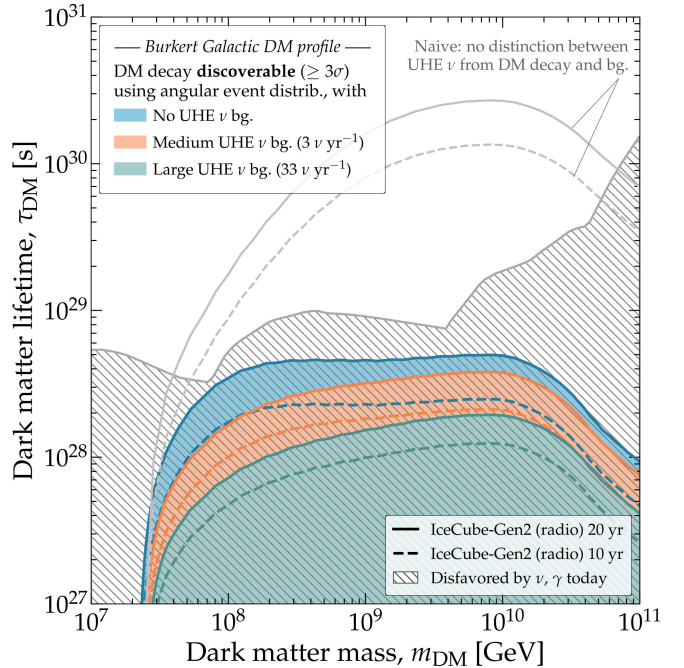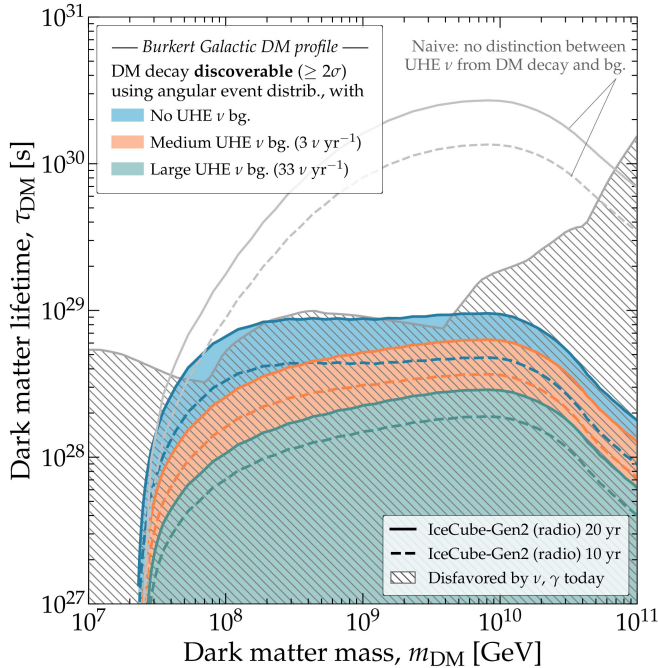

FIG. 16. Discovery prospects for UHE neutrinos from DM decay, using a Burkert Galactic DM profile. Left: for discovery at $\geq 2\sigma$, to be compared with Fig. 7. Right: for discovery at $\geq 3\sigma$, to be compared with Fig. 14.
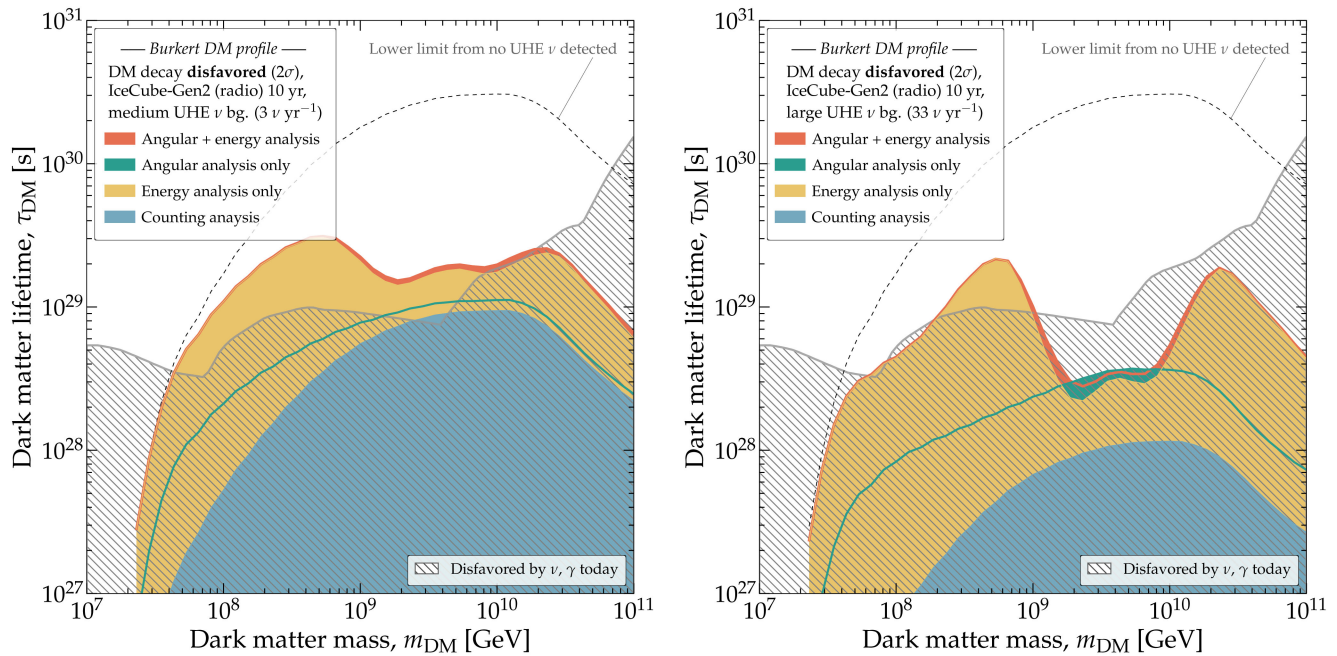
FIG. 17. Projected lower limits on the DM lifetime, using a Burkert Galactic DM profile. Left: for a medium background of non-DM UHE neutrinos, to be compared with Fig. 11. Right: for a large background of non-DM UHE neutrinos, to be compared with Fig. 15.

Figure 14 Discovery prospects at 3σ for the NFW Galactic DM profile.

Figure 15 Lower limits on DM lifetime under a large background of non-DM UHE neutrinos, for the NFW profile.

Figure 16 Discovery prospects at $\geq 2\sigma$ and $\geq 3\sigma$ for the Burkert Galactic DM profile.

Figure 17 Lower limits on DM lifetime for the Burkert Galactic DM profile.

[1] J. H. Oort, The force exerted by the stellar system in the direction perpendicular to the galactic plane and some related problems, Bull. Astron. Inst. Neth. **6**, 249 (1932).

[2] F. Zwicky, Die Rotverschiebung von extragalaktischen Nebeln, Helv. Phys. Acta **6**, 110 (1933); Republished in: Gen. Relativ. Gravit. **41**, 207 (2009).

[3] F. Zwicky, On the masses of nebulae and of clusters of nebulae, Astrophys. J. **86**, 217 (1937).

[4] V. C. Rubin, D. Burstein, W. K. Ford, Jr., and N. Thonnard, Rotation velocities of 16 SA galaxies and a comparison of Sa, Sb, and SC rotation properties, Astrophys. J. **289**, 81 (1985).

[5] K. G. Begeman, A. H. Broeils, and R. H. Sanders, Extended rotation curves of spiral galaxies: Dark haloes and modified dynamics, Mon. Not. R. Astron. Soc. **249**, 523 (1991).

[6] A. G. Bergmann, V. Petrosian, and R. Lynds, Gravitational lens models of arcs in clusters, Astrophys. J. **350**, 23 (1990).

[7] D. Clowe, M. Bradac, A. H. Gonzalez, M. Markevitch, S. W. Randall, C. Jones, and D. Zaritsky, A direct empirical proof of the existence of dark matter, Astrophys. J. Lett. **648**, L109 (2006).

[8] G. F. Smoot *et al.* (COBE Collaboration), Structure in the COBE differential microwave radiometer first year maps, Astrophys. J. Lett. **396**, L1 (1992).

[9] N. Jarosik *et al.* (WMAP Collaboration), Seven-year Wilkinson microwave anisotropy probe (WMAP) observations: Sky maps, systematic errors, and basic results, Astrophys. J. Suppl. Ser. **192**, 14 (2011).

[10] W. J. Percival *et al.* (SDSS Collaboration), Baryon acoustic oscillations in the sloan digital sky survey data release 7 galaxy sample, Mon. Not. R. Astron. Soc. **401**, 2148 (2010).

[11] T. Di Matteo, J. Colberg, V. Springel, L. Hernquist, and D. Sijacki, Direct cosmological simulations of the growth of black holes and galaxies, Astrophys. J. **676**, 33 (2008).

[12] M. Boylan-Kolchin, V. Springel, S. D. M. White, A. Jenkins, and G. Lemson, Resolving cosmic structure formation with the millennium-II simulation, Mon. Not. R. Astron. Soc. **398**, 1150 (2009).

[13] G. Bertone and D. Hooper, History of dark matter, Rev. Mod. Phys. **90**, 045002 (2018).

[14] E. W. Kolb and M. S. Turner, The early universe, Nature (London) **294,** 521 (1981).

[15] K. Griest and M. Kamionkowski, Supersymmetric dark matter, Phys. Rep. **333–334,** 167 (2000).

[16] C. B. Adams *et al.*, Axion Dark Matter, arXiv:2203.14923.

[17] I. Z. Rothstein, K. S. Babu, and D. Seckel, Planck scale symmetry breaking and majoron physics, Nucl. Phys. **B403,** 725 (1993).

[18] V. Berezinsky and J. W. F. Valle, The KeV Majoron as a dark matter particle, Phys. Lett. B **318,** 360 (1993).

[19] T. Brune and H. Päs, Massive Majorons and constraints on the Majoron-neutrino coupling, Phys. Rev. D **99,** 096005 (2019).

[20] A. Boyarsky, M. Drewes, T. Lasserre, S. Mertens, and O. Ruchayskiy, Sterile neutrino dark matter, Prog. Part. Nucl. Phys. **104,** 1 (2019).

[21] B. Carr and F. Kuhnel, Primordial black holes as dark matter candidates, SciPost Phys. Lect. Notes **48,** 1 (2022).

[22] K. Griest and M. Kamionkowski, Unitarity limits on the mass and radius of dark matter particles, Phys. Rev. Lett. **64,** 615 (1990).

[23] J. Smirnov and J. F. Beacom, TeV-scale thermal WIMPs: Unitarity and its consequences, Phys. Rev. D **100,** 043029 (2019).

[24] M. Chianese, D. F. G. Fiorillo, R. Hajjar, G. Miele, S. Morisi, and N. Saviano, Heavy decaying dark matter at future neutrino radio telescopes, J. Cosmol. Astropart. Phys. 05 (2021) 074.

[25] M. G. Aartsen *et al.* (IceCube Collaboration), First observation of PeV-energy neutrinos with IceCube, Phys. Rev. Lett. **111,** 021103 (2013).

[26] M. G. Aartsen *et al.* (IceCube Collaboration), Evidence for high-energy extraterrestrial neutrinos at the IceCube detector, Science **342,** 1242856 (2013).

[27] M. G. Aartsen *et al.* (IceCube Collaboration), Observation of high-energy astrophysical neutrinos in three years of IceCube data, Phys. Rev. Lett. **113,** 101101 (2014).

[28] M. G. Aartsen *et al.* (IceCube Collaboration), Evidence for astrophysical muon neutrinos from the northern sky with IceCube, Phys. Rev. Lett. **115,** 081102 (2015).

[29] M. G. Aartsen *et al.* (IceCube Collaboration), Observation and characterization of a cosmic muon neutrino flux from the northern hemisphere using six years of IceCube data, Astrophys. J. **833,** 3 (2016).

[30] M. Ahlers and F. Halzen, Opening a new window onto the universe with IceCube, Prog. Part. Nucl. Phys. **102,** 73 (2018).

[31] R. Abbasi *et al.* (IceCube Collaboration), The IceCube high-energy starting event sample: Description and flux characterization with 7.5 years of data, Phys. Rev. D **104,** 022002 (2021).

[32] A. Esmaili and P. D. Serpico, Are IceCube neutrinos unveiling PeV-scale decaying dark matter?, J. Cosmol. Astropart. Phys. 11 (2013) 054.

[33] B. Feldstein, A. Kusenko, S. Matsumoto, and T. T. Yanagida, Neutrinos at IceCube from heavy decaying dark matter, Phys. Rev. D **88,** 015004 (2013).

[34] Y. Bai, R. Lu, and J. Salvadó, Geometric compatibility of IceCube TeV-PeV neutrino excess and its galactic dark matter origin, J. High Energy Phys. 01 (2016) 161.

[35] Y. Ema, R. Jinno, and T. Moroi, Cosmic-ray neutrinos from the decay of long-lived particle and the recent IceCube result, Phys. Lett. B **733,** 120 (2014).

[36] A. Esmaili, S. K. Kang, and P. D. Serpico, IceCube events and decaying dark matter: Hints and constraints, J. Cosmol. Astropart. Phys. 12 (2014) 054.

[37] A. Bhattacharya, M. H. Reno, and I. Sarcevic, Reconciling neutrino flux from heavy dark matter decay and recent events at IceCube, J. High Energy Phys. 06 (2014) 110.

[38] K. Murase, R. Laha, S. Ando, and M. Ahlers, Testing the dark matter scenario for PeV neutrinos observed in IceCube, Phys. Rev. Lett. **115,** 071301 (2015).

[39] M. Chianese, G. Miele, S. Morisi, and E. Vitagliano, Low energy IceCube data and a possible dark matter related excess, Phys. Lett. B **757,** 251 (2016).

[40] M. Chianese, G. Miele, and S. Morisi, Dark matter interpretation of low energy IceCube MESE excess, J. Cosmol. Astropart. Phys. 01 (2017) 007.

[41] M. Chianese, G. Miele, and S. Morisi, Interpreting IceCube 6-year HESE data as an evidence for hundred TeV decaying dark matter, Phys. Lett. B **773,** 591 (2017).

[42] A. Bhattacharya, A. Esmaili, S. Palomares-Ruiz, and I. Sarcevic, Update on decaying and annihilating heavy dark matter with the 6-year IceCube HESE data, J. Cosmol. Astropart. Phys. 05 (2019) 051.

[43] M. Chianese, D. F. G. Fiorillo, G. Miele, S. Morisi, and O. Pisanti, Decaying dark matter at IceCube and its signature on high energy gamma experiments, J. Cosmol. Astropart. Phys. 11 (2019) 046.

[44] K. Murase and J. F. Beacom, Constraining very heavy dark matter using diffuse backgrounds of neutrinos and cascaded gamma rays, J. Cosmol. Astropart. Phys. 10 (2012) 043.

[45] K. Murase, D. Guetta, and M. Ahlers, Hidden cosmic-ray accelerators as an origin of TeV-PeV cosmic neutrinos, Phys. Rev. Lett. **116,** 071101 (2016).

[46] A. Capanema, A. Esmaili, and K. Murase, New constraints on the origin of medium-energy neutrinos observed by IceCube, Phys. Rev. D **101,** 103012 (2020).

[47] A. Capanema, A. Esmaili, and P. D. Serpico, Where do IceCube neutrinos come from? Hints from the diffuse gamma-ray flux, J. Cosmol. Astropart. Phys. 02 (2021) 037.

[48] C. A. Argüelles, D. Delgado, A. Friedlander, A. Kheirandish, I. Safa, A. C. Vincent, and H. White, Dark matter decay to neutrinos, arXiv:2210.01303.

[49] R. Abbasi *et al.* (IceCube Collaboration), Searches for connections between dark matter and high-energy neutrinos with IceCube, J. Cosmol. Astropart. Phys. 10 (2023) 003.

[50] R. Abbasi *et al.* (IceCube Collaboration), Search for neutrino lines from dark matter annihilation and decay with IceCube, arXiv:2303.13663.

[51] T. Cohen, K. Murase, N. L. Rodd, B. R. Safdi, and Y. Soreq, γ-ray constraints on decaying dark matter and implications for IceCube, Phys. Rev. Lett. **119,** 021102 (2017).

[52] Z. Cao *et al.* (LHAASO Collaboration), Constraints on heavy decaying dark matter from 570 days of LHAASO observations, Phys. Rev. Lett. **129,** 261103 (2022).

[53] V. S. Berezinsky and G. T. Zatsepin, Cosmic rays at ultrahigh-energies (neutrino?), Phys. Lett. B **28**, 423 (1969).

[54] A. Aab *et al.* (Pierre Auger Collaboration), The Pierre Auger Observatory Upgrade—preliminary design report, arXiv:1604.03637.

[55] S. Wissel *et al.*, Prospects for high-elevation radio detection of > 100 PeV tau neutrinos, J. Cosmol. Astropart. Phys. 11 (2020) 065.

[56] J. H. Adams *et al.*, White paper on EUSO-SPB2, arXiv:1703.04513.

[57] J. R. Hörandel (GCOS Collaboration), GCOS—the global cosmic ray observatory, Proc. Sci., ICRC2021 (**2021**) 027 [arXiv:2203.01127].

[58] J. Álvarez-Muñiz *et al.* (GRAND Collaboration), The giant radio array for neutrino detection (GRAND): Science and design, Sci. China Phys. Mech. Astron. **63**, 219501 (2020).

[59] A. V. Olinto *et al.* (POEMMA Collaboration), The POEMMA (probe of extreme multi-messenger astrophysics) observatory, J. Cosmol. Astropart. Phys. 06 (2021) 007.

[60] C. Deaconu (ANITA Collaboration), Searches for ultrahigh energy neutrinos with ANITA, Proc. Sci., ICRC2019 (**2020**) 867 [arXiv:1908.00923].

[61] J. A. Aguilar *et al.* (RNO-G Collaboration), Design and sensitivity of the radio neutrino observatory in greenland (RNO-G), J. Instrum. **16**, P03025 (2021); **18**, E03001(E) (2023).

[62] J. Nam *et al.*, High-elevation synoptic radio array for detection of upward moving air-showers, deployed in the Antarctic mountains, Proc. Sci., ICRC2019 (**2020**) 967.

[63] M. G. Aartsen *et al.* (IceCube-Gen2 Collaboration), IceCube-Gen2: The window to the extreme Universe, J. Phys. G **48**, 060501 (2021).

[64] M. Ackermann *et al.*, Astrophysics uniquely enabled by observations of high-energy cosmic neutrinos, Bull. Am. Astron. Soc. **51**, 185 (2019).

[65] M. Ackermann *et al.*, High-energy and ultra-high-energy neutrinos: A snowmass white paper, J. High Energy Astrophys. **36**, 55 (2022).

[66] R. Alves Batista *et al.*, EuCAPT white paper: Opportunities and challenges for theoretical astroparticle physics in the next decade, arXiv:2110.10074.

[67] M. Ackermann *et al.*, Fundamental physics with high-energy cosmic neutrinos, Bull. Am. Astron. Soc. **51**, 215 (2019).

[68] C. A. Argüelles, M. Bustamante, A. Kheirandish, S. Palomares-Ruiz, J. Salvadó, and A. C. Vincent, Fundamental physics with high-energy cosmic neutrinos today and in the future, Proc. Sci., ICRC2019 (**2020**) 849 [arXiv:1907.08690].

[69] J. M. Berryman *et al.*, Neutrino self-interactions: A white paper, Phys. Dark Universe **42**, 101267 (2023).

[70] R. Mammen Abraham *et al.*, Tau neutrinos in the next decade: from GeV to EeV, J. Phys. G **49**, 110501 (2022).

[71] C. Guépin, R. Aloisio, L. A. Anchordoqui, A. Cummings, J. F. Krizmanic, A. V. Olinto, M. H. Reno, and T. M. Venters, Indirect dark matter searches at ultrahigh energy neutrino detectors, Phys. Rev. D **104**, 083002 (2021).

[72] K. Greisen, End to the cosmic ray spectrum?, Phys. Rev. Lett. **16**, 748 (1966).

[73] G. T. Zatsepin and V. A. Kuzmin, Upper limit of the spectrum of cosmic rays, JETP Lett. **4**, 78 (1966).

[74] V. B. Valera, M. Bustamante, and C. Glaser, Near-future discovery of the diffuse flux of ultrahigh-energy cosmic neutrinos, Phys. Rev. D **107**, 043019 (2023).

[75] M. Ahlers and K. Murase, Probing the galactic origin of the IceCube excess with gamma-rays, Phys. Rev. D **90**, 023010 (2014).

[76] M. Ahlers, Y. Bai, V. Barger, and R. Lu, Galactic neutrinos in the TeV to PeV range, Phys. Rev. D **93**, 013009 (2016).

[77] A. Neronov and D. V. Semikoz, Evidence for the galactic contribution to the IceCube astrophysical neutrino flux, Astropart. Phys. **75**, 60 (2016).

[78] J. M. Carceller and M. Masip, Diffuse flux of galactic neutrinos and gamma rays, J. Cosmol. Astropart. Phys. 03 (2017) 013.

[79] A. Neronov and D. Semikoz, Galactic and extragalactic contributions to the astrophysical muon neutrino signal, Phys. Rev. D **93**, 123002 (2016).

[80] P. B. Denton, D. Marfatia, and T. J. Weiler, The galactic contribution to IceCube's astrophysical neutrino flux, J. Cosmol. Astropart. Phys. 08 (2017) 033.

[81] M. G. Aartsen *et al.* (IceCube Collaboration), Search for PeV gamma-ray emission from the southern hemisphere with 5 years of data from the IceCube observatory, Astrophys. J. **891**, 9 (2019).

[82] A. Kheirandish, Identifying galactic sources of high-energy neutrinos, Astrophys. Space Sci. **365**, 108 (2020).

[83] G. S. Vance, K. L. Emig, C. Lunardini, and R. A. Windhorst, Searching for a galactic component in the IceCube track-like neutrino events, arXiv:2108.01805.

[84] Y. Y. Kovalev, A. V. Plavin, and S. V. Troitsky, Galactic contribution to the high-energy neutrino flux found in track-like IceCube events, Astrophys. J. Lett. **940**, L41 (2022).

[85] T. Sudoh and J. F. Beacom, Where are Milky Way's hadronic PeVatrons?, Phys. Rev. D **107**, 043002 (2023).

[86] P. De la Torre Luque, D. Gaggero, D. Grasso, and A. Marinelli, Prospects for detection of a galactic diffuse neutrino flux, Front. Astron. Space Sci. **9**, 1041838 (2022).

[87] T. Sudoh and J. F. Beacom, Identifying extended PeVatron sources via neutrino shower detection, Phys. Rev. D **108**, 043016 (2023).

[88] M. Ackermann *et al.* (IceCube Collaboration), Observation of high-energy neutrinos from the galactic plane, Science **380**, 1338 (2023).

[89] V. B. Valera, M. Bustamante, and C. Glaser, The ultra-high-energy neutrino-nucleon cross section: measurement forecasts for an era of cosmic EeV-neutrino discovery, J. High Energy Phys. 06 (2022) 105.

[90] D. F. G. Fiorillo, M. Bustamante, and V. B. Valera, Near-future discovery of point sources of ultra-high-energy neutrinos, J. Cosmol. Astropart. Phys. 03 (2023) 026.

[91] M. G. Aartsen *et al.* (IceCube Collaboration), Differential limit on the extremely-high-energy cosmic neutrino flux in the presence of astrophysical background from nine years of IceCube data, Phys. Rev. D **98**, 062003 (2018).

[92] W. D. Apel *et al.* (KASCADE Grande Collaboration), KASCADE-grande limits on the isotropic diffuse

gamma-ray flux between 100 TeV and 1 EeV, Astrophys. J. **848,** 1 (2017).

[93] R. U. Abbasi *et al.* (Telescope Array Collaboration), Constraints on the diffuse photon flux with energies above 10^{18} eV using the surface detector of the telescope array experiment, Astropart. Phys. **110,** 8 (2019).

[94] D. Veberic, ed., *The Pierre Auger Observatory: Contributions to the 35th International Cosmic Ray Conference (ICRC 2017)* (2017), D. VebericarXiv:1708.06592.

[95] S. H. Margolis, D. N. Schramm, and R. Silberberg, Ultrahigh-energy neutrino astronomy, Astrophys. J. **221,** 990 (1978).

[96] F. W. Stecker, Diffuse fluxes of cosmic high-energy neutrinos, Astrophys. J. **228,** 919 (1979).

[97] S. R. Kelner, F. A. Aharonian, and V. V. Bugayov, Energy spectra of gamma-rays, electrons and neutrinos produced at proton-proton interactions in the very high energy regime, Phys. Rev. D **74,** 034018 (2006); **79,** 039901(E) (2009).

[98] A. Mücke, R. Engel, J. P. Rachen, R. J. Protheroe, and T. Stanev, SOPHIA: Monte Carlo simulations of photohadronic processes in astrophysics, Comput. Phys. Commun. **124,** 290 (2000).

[99] S. Hümmer, M. Ruger, F. Spanier, and W. Winter, Simplified models for photohadronic interactions in cosmic accelerators, Astrophys. J. **721,** 630 (2010).

[100] K. Fang and M. C. Miller, A new method for finding point sources in high-energy neutrino data, Astrophys. J. **826,** 102 (2016).

[101] K. Fang, K. Kotera, M. C. Miller, K. Murase, and F. Oikonomou, Identifying ultrahigh-energy cosmic-ray accelerators with future ultrahigh-energy neutrino detectors, J. Cosmol. Astropart. Phys. 12 (2016) 017.

[102] R. Alves Batista *et al.*, Open questions in cosmic-ray research at ultrahigh energies, Front. Astron. Space Sci. **6,** 23 (2019).

[103] A. Anker *et al.*, White Paper: ARIANNA-200 high energy neutrino telescope, arXiv:2004.09841.

[104] R. Abbasi *et al.* (IceCube Collaboration), Improved characterization of the astrophysical muon–neutrino flux with 9.5 years of IceCube data, Astrophys. J. **928,** 50 (2022).

[105] R. Aloisio, V. Berezinsky, and A. Gazizov, Ultra high energy cosmic rays: The disappointing model, Astropart. Phys. **34,** 620 (2011).

[106] K. Kotera, D. Allard, and A. V. Olinto, Cosmogenic neutrinos: Parameter space and detectabilty from PeV to ZeV, J. Cosmol. Astropart. Phys. 10 (2010) 013.

[107] M. Ahlers and F. Halzen, Minimal cosmogenic neutrinos, Phys. Rev. D **86,** 083010 (2012).

[108] K. Fang, K. Kotera, K. Murase, and A. V. Olinto, Testing the newborn pulsar origin of ultrahigh energy cosmic rays with EeV neutrinos, Phys. Rev. D **90,** 103005 (2014); **92,** 129901(E) (2015).

[109] P. Padovani, M. Petropoulou, P. Giommi, and E. Resconi, A simplified view of blazars: The neutrino background, Mon. Not. R. Astron. Soc. **452,** 1877 (2015).

[110] K. Fang and K. Murase, Linking high-energy cosmic particles by black hole jets embedded in large-scale structures, Nat. Phys. **14,** 396 (2018).

[111] A. Romero-Wolf and M. Ave, Bayesian inference constraints on astrophysical production of ultra-high energy cosmic rays and cosmogenic neutrino flux predictions, J. Cosmol. Astropart. Phys. 07 (2018) 025.

[112] R. Alves Batista, R. M. de Almeida, B. Lago, and K. Kotera, Cosmogenic photon and neutrino fluxes in the Auger era, J. Cosmol. Astropart. Phys. 01 (2019) 002.

[113] J. Heinze, A. Fedynitch, D. Boncioli, and W. Winter, A new view on Auger data and cosmogenic neutrinos in light of different nuclear disintegration and air-shower models, Astrophys. J. **873,** 88 (2019).

[114] M. S. Muzio, M. Unger, and G. R. Farrar, Progress towards characterizing ultrahigh energy cosmic ray sources, Phys. Rev. D **100,** 103008 (2019).

[115] X. Rodrigues, J. Heinze, A. Palladino, A. van Vliet, and W. Winter, Active galactic nuclei jets as the origin of ultrahigh-energy cosmic rays and perspectives for the detection of astrophysical source neutrinos at EeV energies, Phys. Rev. Lett. **126,** 191101 (2021).

[116] M. S. Muzio, G. R. Farrar, and M. Unger, Probing the environments surrounding ultrahigh energy cosmic ray accelerators and their implications for astrophysical neutrinos, Phys. Rev. D **105,** 023022 (2022).

[117] K. Mannheim, High-energy neutrinos from extragalactic jets, Astropart. Phys. **3,** 295 (1995).

[118] A. M. Atoyan and C. D. Dermer, High-energy neutrinos from photomeson processes in blazars, Phys. Rev. Lett. **87,** 221102 (2001).

[119] A. M. Atoyan and C. D. Dermer, Neutral beams from blazar jets, Astrophys. J. **586,** 79 (2003).

[120] J. Álvarez-Muñiz and P. Mészáros, High energy neutrinos from radio-quiet AGNs, Phys. Rev. D **70,** 123001 (2004).

[121] K. Murase, Y. Inoue, and C. D. Dermer, Diffuse neutrino intensity from the inner jets of active galactic nuclei: Impacts of external photon fields and the blazar sequence, Phys. Rev. D **90,** 023007 (2014).

[122] S. S. Kimura, K. Murase, and K. Toma, Neutrino and cosmic-ray emission and cumulative background from radiatively inefficient accretion flows in low-luminosity active galactic nuclei, Astrophys. J. **806,** 159 (2015).

[123] A. Palladino, X. Rodrigues, S. Gao, and W. Winter, Interpretation of the diffuse astrophysical neutrino flux in terms of the blazar sequence, Astrophys. J. **871,** 41 (2019).

[124] C. Righi, A. Palladino, F. Tavecchio, and F. Vissani, EeV astrophysical neutrinos from flat spectrum radio quasars, Astron. Astrophys. **642,** A92 (2020).

[125] S. S. Kimura, K. Murase, and P. Mészáros, Soft gamma rays from low accreting supermassive black holes and connection to energetic neutrinos, Nat. Commun. **12,** 5615 (2021).

[126] A. Neronov and D. Semikoz, Radio-to-gamma-ray synchrotron and neutrino emission from proton–proton interactions in active galactic nuclei, JETP Lett. **113,** 69 (2021).

[127] B. Paczynski and G.-H. Xu, Neutrino bursts from gamma-ray bursts, Astrophys. J. **427,** 708 (1994).

[128] E. Waxman and J. N. Bahcall, High-energy neutrinos from cosmological gamma-ray burst fireballs, Phys. Rev. Lett. **78,** 2292 (1997).

[129] K. Murase, K. Ioka, S. Nagataki, and T. Nakamura, High energy neutrinos and cosmic-rays from low-luminosity gamma-ray bursts?, Astrophys. J. Lett. **651**, L5 (2006).

[130] M. Bustamante, P. Baerwald, K. Murase, and W. Winter, Neutrino and cosmic-ray emission from multiple internal shocks in gamma-ray bursts, Nat. Commun. **6**, 6783 (2015).

[131] N. Senno, K. Murase, and P. Mészáros, Choked jets and low-luminosity gamma-ray bursts as hidden neutrino sources, Phys. Rev. D **93**, 083003 (2016).

[132] T. Pitik, I. Tamborra, and M. Petropoulou, Neutrino signal dependence on gamma-ray burst emission mechanism, J. Cosmol. Astropart. Phys. 05 (2021) 034.

[133] A. Rudolph, M. Petropoulou, W. Winter, and v. Bošnjak, Multi-messenger model for the prompt emission from GRB 221009A, Astrophys. J. Lett. **944**, L34 (2023).

[134] A. Rudolph, M. Petropoulou, v. Bošnjak, and W. Winter, Multicollision internal shock lepto-hadronic models for energetic gamma-ray bursts (GRBs), Astrophys. J. **950**, 28 (2023).

[135] K. Fang, High-energy neutrino signatures of newborn pulsars in the local universe, J. Cosmol. Astropart. Phys. 06 (2015) 004.

[136] G. R. Farrar and A. Gruzinov, Giant AGN flares and cosmic ray bursts, Astrophys. J. **693**, 329 (2009).

[137] X.-Y. Wang, R.-Y. Liu, Z.-G. Dai, and K. S. Cheng, Probing the tidal disruption flares of massive black holes with high-energy neutrinos, Phys. Rev. D **84**, 081301 (2011).

[138] L. Dai and K. Fang, Can tidal disruption events produce the IceCube neutrinos?, Mon. Not. R. Astron. Soc. **469**, 1354 (2017).

[139] N. Senno, K. Murase, and P. Mészáros, High-energy neutrino flares from x-ray bright and dark tidal disruption events, Astrophys. J. **838**, 3 (2017).

[140] C. Lunardini and W. Winter, High energy neutrinos from the tidal disruption of stars, Phys. Rev. D **95**, 123001 (2017).

[141] B. T. Zhang, K. Murase, F. Oikonomou, and Z. Li, High-energy cosmic ray nuclei from tidal disruption events: Origin, survival, and implications, Phys. Rev. D **96**, 063007 (2017); **96**, 069902(A) (2017).

[142] C. Guépin, K. Kotera, E. Barausse, K. Fang, and K. Murase, Ultra-high energy cosmic rays and neutrinos from tidal disruptions by massive black holes, Astron. Astrophys. **616**, A179 (2018); **636**, C3(E) (2020).

[143] W. Winter and C. Lunardini, A concordance scenario for the observed neutrino from a tidal disruption event, Nat. Astron. **5**, 472 (2021).

[144] W. Winter and C. Lunardini, Interpretation of the observed neutrino emission from three tidal disruption events, Astrophys. J. **948**, 42 (2023).

[145] Y. Tsunesada, T. Abuzayyad, D. Ivanov, G. Thomson, T. Fujii, and D. Ikeda, Energy spectrum of ultra-high-energy cosmic rays measured by the telescope array, Proc. Sci., ICRC2017 (**2018**) 535.

[146] D. Bergman and T. Stroman, Telescope array measurement of UHECR composition from stereoscopic fluorescence detection, Proc. Sci., ICRC2017 (**2018**) 538.

[147] A. Aab *et al.* (Pierre Auger Collaboration), Probing the origin of ultra-high-energy cosmic rays with neutrinos in the EeV energy range using the Pierre Auger Observatory, J. Cosmol. Astropart. Phys. 10 (2019) 022.

[148] M. Chianese, D. F. G. Fiorillo, R. Hajjar, G. Miele, and N. Saviano, Constraints on heavy decaying dark matter with current gamma-ray measurements, J. Cosmol. Astropart. Phys. 11 (2021) 035.

[149] R. Abbasi *et al.* (IceCube-Gen2 Collaboration), Sensitivity studies for the IceCube-Gen2radio array, Proc. Sci., ICRC2021 (**2021**) 1183 [arXiv:2107.08910].

[150] C. J. Hogan and J. J. Dalcanton, New dark matter physics: Clues from halo structure, Phys. Rev. D **62**, 063511 (2000).

[151] P. Bode, J. P. Ostriker, and N. Turok, Halo formation in warm dark matter models, Astrophys. J. **556**, 93 (2001).

[152] S. Das, K. Murase, and T. Fujii, Revisiting ultrahigh-energy constraints on decaying superheavy dark matter, Phys. Rev. D **107**, 103013 (2023).

[153] C. W. Bauer, N. L. Rodd, and B. R. Webber, Dark matter spectra from the electroweak to the Planck scale, J. High Energy Phys. 06 (2021) 121.

[154] P. Ciafaloni, D. Comelli, A. Riotto, F. Sala, A. Strumia, and A. Urbano, Weak corrections are relevant for dark matter indirect detection, J. Cosmol. Astropart. Phys. 03 (2011) 019.

[155] J. F. Navarro, C. S. Frenk, and S. D. M. White, The structure of cold dark matter halos, Astrophys. J. **462**, 563 (1996).

[156] J. Einasto, Kinematics and dynamics of stellar systems, Tr. Astrofiz. Inst. Alma-Ata **5**, 87 (1965).

[157] A. Burkert, The Structure of dark matter halos in dwarf galaxies, Astrophys. J. Lett. **447**, L25 (1995).

[158] M. Cirelli, G. Corcella, A. Hektor, G. Hutsi, M. Kadastik, P. Panci, M. Raidal, F. Sala, and A. Strumia, PPPC 4 DM ID: A poor particle physicist cookbook for dark matter indirect detection, J. Cosmol. Astropart. Phys. 03 (2011) 051; 10 (2012) E01.

[159] R. Gandhi, C. Quigg, M. H. Reno, and I. Sarcevic, Neutrino interactions at ultrahigh-energies, Phys. Rev. D **58**, 093009 (1998).

[160] R. Brock *et al.* (CTEQ Collaboration), Handbook of perturbative QCD: Version 1.0, Rev. Mod. Phys. **67**, 157 (1995).

[161] J. M. Conrad, M. H. Shaevitz, and T. Bolton, Precision measurements with high-energy neutrino beams, Rev. Mod. Phys. **70**, 1341 (1998).

[162] J. A. Formaggio and G. P. Zeller, From eV to EeV: Neutrino cross sections across energy scales, Rev. Mod. Phys. **84**, 1307 (2012).

[163] M. G. Aartsen *et al.* (IceCube Collaboration), Measurement of the multi-TeV neutrino cross section with IceCube using Earth absorption, Nature (London) **551**, 596 (2017).

[164] M. Bustamante and A. Connolly, Extracting the energy-dependent neutrino-nucleon cross section above 10 TeV using IceCube showers, Phys. Rev. Lett. **122**, 041101 (2019).

[165] M. G. Aartsen *et al.* (IceCube Collaboration), Measurements using the inelasticity distribution of multi-TeV

neutrino interactions in IceCube, Phys. Rev. D **99**, 032004 (2019).

[166] R. Abbasi *et al.* (IceCube Collaboration), Measurement of the high-energy all-flavor neutrino-nucleon cross section with IceCube, Phys. Rev. D **104**, 022001 (2020).

[167] A. García, R. Gauld, A. Heijboer, and J. Rojo, Complete predictions for high-energy neutrino propagation in matter, J. Cosmol. Astropart. Phys. 09 (2020) 025.

[168] A. García, R. Gauld, A. Heijboer, J. Rojo, and V. B. Valera, https://github.com/pochoarus/NuPropEarth (2021), NuPropEarth.

[169] A. M. Dziewonski and D. L. Anderson, Preliminary reference earth model, Phys. Earth Planet. Interiors **25**, 297 (1981).

[170] E. Zas, F. Halzen, and T. Stanev, Electromagnetic pulses from high-energy showers: Implications for neutrino detection, Phys. Rev. D **45**, 362 (1992).

[171] G. A. Askar'yan, Excess negative charge of an electron-photon shower and its coherent radio emission, Zh. Eksp. Teor. Fiz. **41**, 616 (1961).

[172] F. G. Schröder, Radio detection of cosmic-ray air showers and high-energy neutrinos, Prog. Part. Nucl. Phys. **93**, 1 (2017).

[173] S. Barwick and C. Glaser, Radio detection of high energy neutrinos in Ice, arXiv:2208.04971.

[174] C. Guépin, K. Kotera, and F. Oikonomou, High-energy neutrino transients and the future of multi-messenger astronomy, Nat. Rev. Phys. **4**, 697 (2022).

[175] D. García-Fernández, A. Nelles, and C. Glaser, Signatures of secondary leptons in radio-neutrino detectors in ice, Phys. Rev. D **102**, 083011 (2020).

[176] C. Glaser *et al.*, NuRadioMC: Simulating the radio emission of neutrinos from interaction to detector, Eur. Phys. J. C **80**, 77 (2020).

[177] C. Glaser, A. Nelles, I. Plaisier, C. Welling, S. W. Barwick, D. García-Fernández, G. Gaswint, R. Lahmann, and C. Persichilli, NuRadioReco: A reconstruction framework for radio neutrino detectors, Eur. Phys. J. C **79**, 464 (2019).

[178] J. A. Aguilar *et al.*, Reconstructing the neutrino energy for in-ice radio detectors: A study for the radio neutrino observatory greenland (RNO-G), Eur. Phys. J. C **82**, 147 (2022).

[179] S. Stjärnholm, O. Ericsson, and C. Glaser, Neutrino direction and flavor reconstruction from radio detector data using deep convolutional neural networks, Proc. Sci., ICRC2021 (**2021**) 1055.

[180] C. Glaser, D. García-Fernández, and A. Nelles, Prospects for neutrino-flavor physics with in-ice radio detectors, Proc. Sci., ICRC2021 (**2021**) 1231.

[181] G. Cowan, K. Cranmer, E. Gross, and O. Vitells, Asymptotic formulae for likelihood-based tests of new physics, Eur. Phys. J. C **71**, 1554 (2011); **73**, 2501(E) (2013).

[182] S. S. Wilks, The large-sample distribution of the likelihood ratio for testing composite hypotheses, Ann. Math. Stat. **9**, 60 (1938).

[183] I. Esteban, M. C. González-García, M. Maltoni, T. Schwetz, and A. Zhou, The fate of hints: Updated global analysis of three-flavor neutrino oscillations, J. High Energy Phys. 09 (2020) 178.

[184] I. Esteban, M. C. González-García, M. Maltoni, T. Schwetz, and A. Zhou, http://www.nu-fit.org/ (2020), NuFit 5.0.

[185] N. Song, S. W. Li, C. A. Argüelles, M. Bustamante, and A. C. Vincent, The future of high-energy astrophysical neutrino flavor measurements, J. Cosmol. Astropart. Phys. 04 (2021) 054.

[186] M. Bustamante, J. F. Beacom, and W. Winter, Theoretically palatable flavor combinations of astrophysical neutrinos, Phys. Rev. Lett. **115**, 161302 (2015).

[187] J. van Santen, B. A. Clark, R. Halliday, S. Hallmann, and A. Nelles, toise: A framework to describe the performance of high-energy neutrino detectors, J. Instrum. **17**, T08009 (2022).